

Assessing formic and acetic acid emissions and chemistry in western U.S. wildfire smoke: implications for atmospheric modeling

Wade Permar¹, Catherine Wielgasz¹, Lixu Jin¹, Xin Chen², Matthew M. Coggon³, Lauren A. Garofalo⁴, Georgios I. Gkatzelis⁵, Damien Ketcherside¹, Dylan B. Millet², Brett B. Palm⁶, Qiaoyun Peng⁷, Michael A. Robinson³, Joel A. Thornton⁷, Robert J. Yokelson¹, Patrick Veres³, Carsten Warneke³, Emily V. Fischer⁸, Lu Hu¹

¹Department of Chemistry and Biochemistry, University of Montana, Missoula, MT, USA.

²Department of Soil, Water, and Climate, University of Minnesota, St. Paul, MN, USA.

³Chemical Sciences Laboratory, National Oceanic and Atmospheric Administration, Boulder, CO, USA.

⁴Department of Chemistry, Colorado State University, Fort Collins, CO, USA.

⁵Institute of Energy and Climate Research, IEK-8: Troposphere, Forschungszentrum Jülich GmbH, Jülich, Germany.

⁶Atmospheric Chemistry Observations & Modeling Laboratory, National Center for Atmospheric Research, Boulder, CO, USA.

⁷Department of Atmospheric Sciences, University of Washington, Seattle, WA, USA.

⁸Department of Atmospheric Science, Colorado State University, Fort Collins, CO, USA.

Correspondence: Wade Permar (wade.permar@umontana.edu)

1 Abstract

2 Formic acid (FA) and acetic acid (AA), two of the most abundant organic acids in the
3 atmosphere, are typically underestimated by atmospheric models. Here we investigate their
4 emissions, chemistry, and measurement uncertainties in biomass burning smoke sampled during
5 the WE-CAN and FIREX-AQ aircraft campaigns. Our observed FA emission ratios (ERs) and
6 emission factors (EFs) were generally higher than the 75th percentile of literature values, with
7 little dependence on fuel type or combustion efficiency. Rapid in-plume FA production was
8 observed ($2.7 \text{ ppb ppm}_{\text{CO}}^{-1} \text{ h}^{-1}$), representing up to ~20 % of the total emitted carbon being
9 converted to FA within half a day.

10

11 AA ERs and EFs showed good agreement with the literature, with little or no secondary
12 production observed within < 8 hours of plume aging. Observed FA and AA trends in the near-
13 field were not captured by a box model using the explicit Master Chemical Mechanism nor
14 simplified GEOS-Chem chemistry, even after tripling the model's initial VOC conditions.
15 Consequently, the GEOS-Chem chemical transport model underestimates both acids in the

16 western U.S. by a factor of > 4. This is likely due to missing secondary chemistry in biomass
17 burning smoke and/or coniferous forest biogenic emissions. This work highlights uncertainties in
18 measurements (up to 100%) and even large unknowns in the chemical formation of organic acids
19 in polluted environments, both of which need to be addressed to better understand their global
20 budget.

21 **1 Introduction**

22 Formic acid (FA) and acetic acid (AA) are the two most prevalent organic acids in the
23 troposphere, affecting aqueous-phase chemistry¹ and gas-aerosol partitioning² by regulating pH
24 levels in cloud droplets and aerosols.^{3–6} Multiple studies have shown that various models
25 continuously underestimate both FA and AA abundance compared to ground, airborne, and
26 satellite observations. This low model bias is most pronounced in biogenic source regions,^{7,8}
27 including United States (U.S.) deciduous forests,^{9,10} boreal forests,¹¹ tropical forests,⁶ and in the
28 Arctic tundra.¹² Additionally, models typically fail to capture FA and AA enhancements in
29 plumes from mixed anthropogenic sources^{13,14} and in biomass burning (BB) impacted regions,^{15–}
30 ¹⁷ indicating potential missing primary and/or secondary sources in smoke. In this work, we
31 investigate emissions, secondary productions, and model representations of FA and AA in the
32 western U.S. during two wildfire seasons, using measurements made during the WE-CAN
33 (Western Wildfire Experiment for Cloud Chemistry, Aerosol Absorption, and Nitrogen) and
34 FIREX-AQ (Fire Influence on Regional to Global Environments and Air Quality) field
35 campaigns.

36
37 FA and AA are two of the most abundantly emitted volatile organic compounds (VOCs) from
38 BB, accounting for 16 % of the average VOC emissions by mass in western U.S. wildfires.¹⁸ As
39 smoke plumes age, substantial secondary production of FA and AA may occur,^{19–23} resulting in
40 these compounds together being one of the largest OH sinks in smoke aged more than 3 days,
41 accounting for up to ~25 % of plume OH reactivity.²⁴ Similarly, FA and AA can account for up
42 to 15 % of the VOC OH reactivity in urban atmospheres as well as the clean free troposphere in
43 the western U.S. during wildfire season.²⁴

44
45 Globally, top-down estimates suggest FA sources could reach 100–120 Tg y⁻¹,⁶ which is two to
46 three times higher than the sum of its known sources.^{6,8,16} Of this, photochemical production

47 from biogenic sources has been estimated to contribute up to 90 % of the global FA budget.⁶
48 Biomass burning may account for up to 16 Tg y⁻¹ (~13–16 %) of FA globally,¹⁶ though such
49 estimates for BB are mostly based on direct emissions. The secondary production of FA from BB
50 precursors is poorly known due in part to the high uncertainty in BB emissions and a large
51 amount of reactive BB precursors, such as furan containing species, not being implemented in
52 current chemical transport models (CTMs).²⁴ Similarly, global AA sources have been estimated
53 using a bottom-up approach to be 85 Tg y⁻¹,⁸ which is likely a lower bound.⁷ Despite BB being a
54 major source of AA,^{23–26} the contribution of BB to the global AA budget is rarely discussed in
55 the literature and is not
56 well constrained.

57
58 The primary sinks of atmospheric FA and AA include wet and dry deposition, photochemical
59 oxidation by OH radicals, and the irreversible uptake on dust resulting in atmospheric lifetimes
60 of 2–4 days for FA and ~2 days for AA.^{6–8,27} Consequently, their relatively short atmospheric
61 lifetimes coupled with the localized and seasonal nature of fires likely means BB alone cannot
62 close the global FA and AA budgets.⁸ However, in regions heavily impacted by BB it is likely
63 that fires play an important role in their regional abundance and a more detailed understanding of
64 their emissions and chemistry in wildfire smoke is needed.

65
66 As the two simplest organic acids, FA and AA may be produced from the oxidation of many
67 different VOCs and are known photochemical products of isoprene, terminal alkenes,
68 monoterpenes, glycolaldehyde, aromatics, acetone, and acetaldehyde.^{7,8,14,28–31} Heterogeneous
69 formation of FA in aerosols and cloud droplets has also been identified as a potential major
70 source, which, when included in the global chemistry–climate model ECHAM5/MESSy
71 (EMAC), has been found to largely reconcile the global FA budget.^{32,33} However, regional
72 discrepancies remain. For example, FA abundances were still underestimated in boreal forested
73 regions, likely due to low emissions of FA precursors from BB.³²

74
75 Analytical challenges measuring FA and AA,³⁴ along with an incomplete understanding of
76 chemical processes in smoke,³⁵ has made it difficult to accurately model their evolution in BB
77 plumes.^{16,36} For example, it has been well documented that the GEOS-Chem CTM underpredicts

78 FA and AA abundances. Missing secondary production from biogenic precursors is thought to be
79 one of the most significant reasons for the low model bias,⁷ though in some ecosystems there
80 may still be missing primary emissions and/or in-canopy sources.^{11,37} The overall model sink
81 may also be too large.³⁸ By updating the model chemistry to reflect photochemical FA
82 production from alkynes, monoterpenes, isoprene, methyl peroxy radical (CH₃O₂), ozonolysis of
83 terminal alkenes, keto-enol tautomerization, and phototautomerization of acetaldehyde,^{7,8,39} Chen
84 et al.¹⁷ were able to improve GEOS-Chem representation of the remote free troposphere relative
85 to observations during ATOM. Despite the updated chemistry, the model underestimated the
86 median FA:CO ratio by a factor of >2 and the 95th percentile by a factor of >4,¹⁷ suggesting that
87 there are still significant missing secondary sources in smoke.

88
89 In this work, we examine FA and AA emissions and chemistry in wildfire smoke to better
90 understand the role of BB in their regional budgets. Using observations from the WE-CAN and
91 FIREX-AQ aircraft campaigns, we first assess FA measurements made by two commonly used
92 chemical ionization mass spectrometers, PTR-ToF and I⁻ CIMS (proton-transfer-reaction time-
93 of-flight mass spectrometer and iodide adduct chemical-ionization mass spectrometer).
94 Emissions for FA and AA are then compared with literature values before examining their
95 chemistry during WE-CAN in five pseudo-Lagrangian sampled smoke plumes. Finally, we
96 assess GEOS-Chem representation of both acids across two fire seasons, first using observations
97 made during the WE-CAN field campaign and then FIREX-AQ as an additional test for year-to-
98 year variability and regional representativeness.

99 **2 Methods**

100 **2.1 WE-CAN and FIREX-AQ campaign overviews and sampling approach**

101 Comprehensive gas and aerosol measurements were made in wildfire smoke plumes across seven
102 western U.S. states from 24 July to 13 September 2018 during the WE-CAN aircraft campaign
103 (https://www.eol.ucar.edu/field_projects/we-can). *In situ* smoke plume sampling was carried out
104 aboard the NSF/NCAR C-130 research aircraft based out of Boise, ID, typically between 14:00
105 and 19:00 local time when burning conditions were most active. Figure S1 depicts the C-130
106 flight tracks during WE-CAN, colored by the observed formic and acetic acid mixing ratios.

107 Upon arriving at a fire, the C-130 would typically sample fire emissions by flying perpendicular
108 transects through the plume, as near to the source as was allowed by firefighting operations and
109 plane safety constraints. To investigate plume aging, most plumes were subsequently sampled
110 using a pseudo-Lagrangian approach where perpendicular transects were performed in a stepwise
111 pattern starting near a fire and continuing as far downwind as possible (seen as the zig-zag flight
112 pattern in Figure S1). In total, WE-CAN sampled more than 22 hours of wildfire smoke,
113 including 31 emission transects of 24 unique fires¹⁸ and 1.2 hours of smoke estimated to have
114 aged >3 days, along with 4.8 hours of the clean free troposphere.²⁴

115
116 The FIREX-AQ aircraft campaign sampled BB plumes across the western and southeastern U.S.
117 from 22 July to 5 September 2019 (<https://csl.noaa.gov/projects/firex-aq>) following a similar
118 sampling approach as WE-CAN.⁴⁰ In this work, we separate FIREX-AQ data into its western and
119 southeastern U.S. portions (FIREX-AQ-W and FIREX-AQ-SE), delimited by the 105th
120 meridian west, for a more accurate regional comparison. This allows us to assess FA and AA
121 representation in the GEOS-Chem CTM across multiple fire seasons and regions. As the total
122 VOC emissions in the western U.S. during the 2018 WE-CAN campaign were $\sim 10 \times$ higher,
123 with $\sim 2 \times$ more area burned, than during the 2019 FIREX-AQ campaign (190 GgC vs. 20 GgC,
124 3.5×10^6 ha vs. 1.9×10^6 ha),^{41,42} these two datasets provide complementary representation of a
125 wide range of seasonal fire activity allowing the model to be assessed under varying real-world
126 conditions.

127 **2.2 Measurements of formic acid, acetic acid, and organic aerosol**

128 FA and AA were both measured by two different proton-transfer-reaction time-of-flight mass
129 spectrometers (PTR-ToF) and an iodide adduct chemical-ionization mass spectrometers (I-
130 CIMS) during the WE-CAN and FIREX-AQ campaigns. The PTR-ToF¹⁸ and I- CIMS⁴³⁻⁴⁶
131 operated during WE-CAN and FIREX-AQ^{47,48} and referenced in this work have been extensively
132 described by the cited literature, while here we include those details most relevant to their
133 measurements of FA and AA.

134
135 Organic aerosol (OA) was measured by high-resolution aerosol mass spectrometry (HR-AMS;
136 Aerodyne Inc.), described in detail by Garofalo et al.⁴⁹ During WE-CAN, the HR-AMS

137 measured OA with 5 s time resolution, vacuum aerodynamic diameter of ~70–1,000 nm, and
138 uncertainty of 35%. In this work we primarily use the fractional component of OA attributed to
139 the CO_2^+ ion (f_{44}), an OA oxidation marker.^{50,51} For plume transects, f_{44} averages are weighted
140 by the measured OA mass.⁵²

141

142 **2.2.1 PTR-ToF**

143 During WE-CAN, the PTR-ToF measured at 2 or 5 Hz frequency with drift tube conditions
144 maintained at 3.00 mbar, 810 V, and 60°C, resulting in an E/N of 130 Td. Sampling was done by
145 drawing ambient air into the cabin at 10–15 lpm through ~3 meters of 3.175 mm I.D.
146 perfluoroalkoxy (PFA) tubing, maintained at ~55°C. This sample stream was then subsampled
147 by the PTR-ToF drift tube through ~100 cm of 1.588 mm O.D. PEEK tubing (60°C), resulting in
148 a total inlet residence of less than 2 s. Three-minute instrument zeroes were performed every
149 hour by sampling VOC free air generated via a platinum bead catalyst heated to 375°C.

150

151 Calibrating FA and AA is analytically challenging due to their instability in gas standards and
152 known humidity-dependent sensitivities in PTR-ToF measurements.⁵³ To overcome these
153 challenges, humidity-dependent FA and AA sensitivities were determined in the laboratory post-
154 campaign using a commercial liquid calibration unit (LCU; Ionicon Analytik). Analytical grade
155 FA and AA were volatilized in the LCU and dynamically diluted into zero air where the
156 humidity was varied within the range observed during WE-CAN as determined by the internal
157 humidity proxy of $\text{H}_2\text{O}\cdot\text{H}_3\text{O}^+$ to H_3O^+ ($[m/z\ 39]/[m/z\ 21]$, 0–6 %).^{53,54} The resulting calibration
158 curves for FA and AA sensitivities as a function of the percent $[m/z\ 39]/[m/z\ 21]$ are shown in
159 Figure S2 and applied to all WE-CAN FA and AA PTR-ToF measurements. Note that similar
160 calibrations and humidity corrections were applied to PTR-ToF measurements during FIREX-
161 AQ. Over the 0–6 % $[m/z\ 39]/[m/z\ 21]$ range, sensitivities for both species were observed to
162 decrease with increased humidity, ranging ~9–4 ncps/ppb, similar to the sensitivity change
163 reported by Baasandorj et al.⁵³. During WE-CAN the PTR-ToF FA and AA uncertainties are
164 conservatively estimated as 50 %, mostly due to 40 % potential instrument drift between WE-
165 CAN and the laboratory calibrations as determined from the observed instrument sensitivity

166 change of other gas standards. The detection limits are 1.0 ppb for FA and 0.5 ppb for AA for
167 our 1 Hz measurements, defined as 3σ for the inflight instrument zeros.

168
169 In PTR-ToF, FA (HCOOH) and AA (CH₃COOH) are detected at their protonated masses, m/z
170 47.013 and m/z 61.028 respectively. The corresponding mass resolution during WE-CAN is 2120
171 $m/\Delta m$ at m/z 47 and 3060 $m/\Delta m$ at m/z 61, where Δm is the full width at half maximum for the
172 ion peak. FA has three major potential interfering ions: dimethyl ether (DME, m/z 47.077),
173 ethanol (m/z 47.050), and N₂H₃O⁺ (m/z 47.024).^{25,53} The mass resolution during WE-CAN was
174 high enough to separate DME and ethanol signals from FA, with ethanol abundance also
175 expected to be $\sim 4 \times$ lower than FA in BB smoke with an instrumental sensitivity $\sim 10 \times$ lower
176 than FA.²⁵ The N₂H₃O⁺ signal, which was not fully resolved from FA, was observed to stay
177 constant regardless of emission source strength throughout the campaign and was therefore
178 classified and corrected as instrumental background. Consequently, we treat the m/z 47 signal as
179 being primarily FA in agreement with previous literature.⁵³⁻⁵⁵

180
181 Potential interferences of AA in PTR-TOF measurements include 2-propanol and n-propanol
182 (m/z 61.065), peroxyacetic acid (PAA) fragments (m/z 61.028), ethyl acetate fragments (m/z
183 61.028), methyl formate (m/z 61.028), and glycolaldehyde (m/z 61.028).^{25,53,55-59} Propanol was
184 resolved from AA during WE-CAN, while PAA fragments, ethyl acetate fragments, methyl
185 formate, and glycolaldehyde are all isomeric with AA. PAA is formed by the reaction of
186 CH₃C(O)O₂ radicals with HO₂, which may be important in low NO_x conditions⁵³ but is $\sim 100 \times$
187 less abundant than AA in fresh BB smoke ($\sim 20 \times$ less abundant after 1.5 hours aging)²² making
188 its fragment unlikely to be a significantly contributor to m/z 61.²⁵ Ethyl acetate is used in
189 coatings, adhesives, cosmetics, and as a process solvent,⁶⁰ resulting in it being most prevalent in
190 anthropogenically polluted areas, while it has not been reported in significant quantities in BB
191 emissions.^{25,61} For methyl formate, a small peak can be seen in the GC-MS during the FIREX-
192 AQ laboratory burning experiment, but FTIR comparison suggests its contribution is
193 negligible.²⁵ Due to interference from these isomers being minimal in BB smoke, we do not
194 attempt to correct for their presence, and assume m/z 61 to be predominantly AA and
195 glycolaldehyde in wildfire emissions.⁶²

196

197 Based on the FIREX-AQ Missoula fire laboratory burning experiments, the m/z 61 signal is on
198 average 67 % AA and 33 % glycolaldehyde (± 45 % of value) in fresh BB emissions.^{25,63}
199 However, the glycolaldehyde contribution in aged smoke is not well described. As
200 glycolaldehyde's atmospheric lifetime of 1 day⁶⁴ is approximately half of that of AA⁸, it is likely
201 that m/z 61 becomes more predominantly AA in aged air masses, though glycolaldehyde
202 production could offset its loss. Given that the relative contribution of glycolaldehyde to m/z 61
203 was not constrained during WE-CAN, we do not attempt to correct for the potential
204 glycolaldehyde interference and apply only the humidity dependent AA sensitivity to m/z 61.
205 Though we treat and discuss the PTR-ToF m/z 61 as AA in this work, the reported values reflect
206 the combined AA and glycolaldehyde isomers and therefore likely represent an upper bound for
207 AA.

208

209 **2.2.2 I⁻ CIMS**

210 I⁻ CIMS operates by colliding iodide ions (I⁻) with neutral analytes inside an ion-molecule
211 reaction region (IMR), forming clusters which are then analyzed by a time-of-flight mass
212 spectrometer. During WE-CAN, ambient air was sampled at 20 lpm through a 40 cm long, 18
213 mm O.D. PTFE tube before being subsampled into the IMR. Between the inlet and IMR, the
214 residence time was < 0.7 seconds. Humidity in the IMR was controlled to maintain a constant
215 iodide-water (m/z 145) to iodide (m/z 127) ratio thereby reducing the instruments humidity
216 dependence.

217

218 The I⁻ CIMS employed a fast-zeroing approach described in Palm et al.⁴⁵ where background
219 concentrations were found by sampling ultra-high purity N₂ into the IMR for 6 seconds every
220 minute. The fast zeros were used to determine the background-subtracted signal by isolating the
221 effects of adsorption and desorption of 'sticky' molecules on the internal IMR surfaces. This
222 zero occurred both in and out of smoke plumes to account for the changes in background signal
223 with varying sampled concentrations. A full inlet zero was also performed for 10 seconds every
224 20 minutes to determine the combined background signal from inlet tubing plus IMR surfaces,
225 which confirmed that the dominant source of the background was from the IMR and not inlet
226 tubing.⁴⁵

227
228 The I⁻ CIMS detects FA as a cluster with iodide at m/z 172.911. For WE-CAN, FA was
229 calibrated in the laboratory prior to the campaign by flowing pure air over heated permeation
230 tubes with gravimetrically determined permeation rates. Although I⁻ CIMS measures AA, due to
231 its low sensitivity and apparent interference from an unknown compound during WE-CAN, we
232 only report AA from PTR-ToF. Recent work has shown that one potential source of uncertainty
233 for the I⁻ CIMS FA measurement is that its sensitivity to FA decreases with increasing IMR
234 temperature.⁴⁸ The I⁻ CIMS deployed during WE-CAN did not directly regulate temperature in
235 the IMR. During smoke sampling periods the C-130 cabin temperatures measured near the I⁻
236 CIMS ranged from 20–32 °C (10th and 90th percentiles: 22–26 °C). Robinson et al.⁴⁸ showed that
237 a 10 °C change in IMR temperature could correspond to a 50 % change in sensitivity, though
238 differences in pressures and tuning between instruments makes applying this uncertainty to the
239 WE-CAN deployment highly uncertain. It is also unlikely that the IMR temperature fluctuated as
240 widely as the cabin temperature, though a lack of data makes it difficult to constrain the actual
241 IMR temperature during WE-CAN or during the laboratory calibrations. Consequently, we
242 conservatively estimate the I⁻ CIMS FA measurement to be a likely upper bound, with 60 %
243 uncertainty and 30 ppt detection limit for 1 Hz data, based on calibration uncertainties and
244 potential variation in IMR temperature.

245

246 **2.2.3 FIREX-AQ**

247 the PTR-ToF and I⁻ CIMS deployed during FIREX-AQ had a few notable configuration
248 differences relative to ones used during the WE-CAN deployment. For the PTR-ToF, the inlet
249 was only ~1 m in length and was comprised of 3.175 mm I.D. PTFE heated to ~50–60 °C. The
250 residence time is estimated as less than 1s. The PTR-ToF was calibrated against FA and AA
251 using total carbon methods as described by Veres et al.⁶⁵ with similar humidity dependencies
252 determined following the methods described in Section 2.2.1. The FIREX-AQ PTR-ToF
253 instrument uncertainty is 30 % for FA and 50 % for AA. Note that in this work, we remove all
254 FIREX-AQ PTR-ToF FA observations above ~4.9 km ASL (above sea level, <550 hPa) from
255 our analysis due to a known background issue in the high-altitude FA measurements.

256

257 For the I CIMS, ambient air was sampled at 6 slpm through a mass-flow-controlled PFA inlet
258 (70 cm length, 6.4 mm I. D.) maintained at 40 °C. A pressure control region upstream of a
259 critical orifice at the entrance to the IMR was maintained at 140 mbar, and thus a constant flow
260 of 1.2 slpm ambient air entered the IMR to mix with the 1 slpm ion source flow. Similar to the I-
261 CIMS deployed during WE-CAN, the IMR was humidified to minimize instrument humidity
262 dependence. The instrument background signal was determined in flight by overflowing the inlet
263 with scrubbed ambient air for 30 s every 10 min through a port located 2 cm downstream of the
264 inlet entrance.⁴⁷ IMR temperature was not controlled during FIREX-AQ, but a post campaign
265 temperature correction was applied to the data as described in Robinson et al.⁴⁸ The instrument
266 uncertainty for FA is 15% + 30 ppt with a 3-sigma detection limit of 6 ppt.

267

268 **2.3 GEOS-Chem chemical transport model**

269 GEOS-Chem nested grid simulations (version 12.1.1)^{66,67} over North America were run for the
270 WE-CAN and FIREX-AQ periods using the model conditions described in Chen et al.¹⁷
271 Simulations were carried out using Goddard Earth Observation System Forward Processing
272 (GEOS-FP) assimilated meteorology data with detailed HO_x, NO_x, VOC, ozone, halogen, and
273 aerosol chemistry. Model runs were conducted at 0.25° × 0.3125° (~25 km) resolution with time
274 steps of 5 min (transport/convection) and 10 min (chemistry/emission). Emissions follow Chen
275 et al.¹⁷ with the notable exception that we use Global Fire Assimilation System version 1.2
276 (GFAS) BB emissions with FA and AA emission ratios updated based on Permar et al.,¹⁸ which
277 in turn reflect the WE-CAN averages discussed in Section 4. GEOS-Chem was subsequently
278 sampled along both campaign flight tracks for comparison to the observations.

279

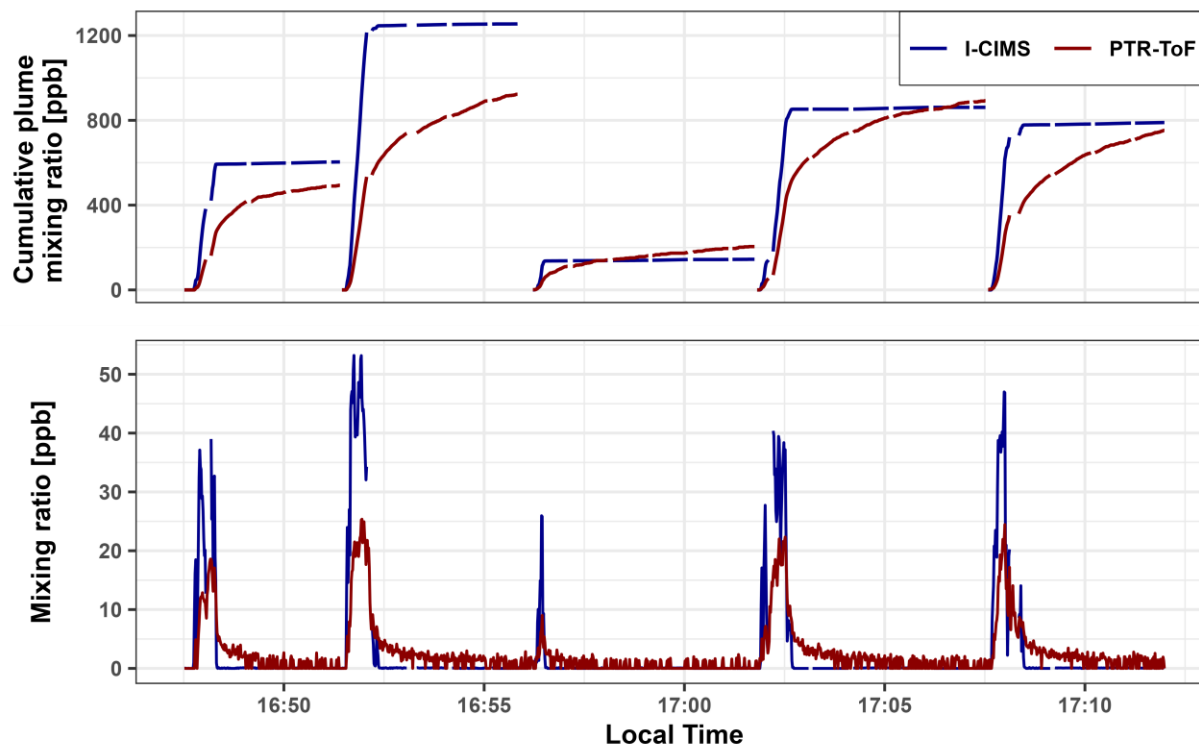
280 The GEOS-Chem simulations also reflect updated FA chemistry including photochemical FA
281 production based on OH initiated oxidation of alkynes, monoterpenes, isoprene, and CH₃O₂,
282 ozonolysis of terminal alkenes (e.g. ethene, propene, isoprene), keto-enol tautomerization,^{7,8}
283 and phototautomerization of acetaldehyde.³⁹ The model does not included the aerosol chemistry
284 proposed by Franco et al.³² Based on these updates, Chen et al.¹⁷ found that GEOS-Chem
285 accurately simulated FA concentrations in the remote free troposphere during the Atmospheric
286 Tomography (ATom) aircraft campaign, indicating that GEOS-Chem is not missing any

287 significant FA sources in the remote free troposphere. The model was found to significantly
288 underestimate FA mixing ratios in 1–10 day aged plumes attributed to both anthropogenic and
289 BB sources. In this work, we investigate how well GEOS-Chem, with the Chen et al.¹⁷ treatment
290 of FA and AA chemistry, represents these acids in the western U.S. under heavily smoke
291 impacted conditions.

292 **3 Formic acid measurement intercomparison**

293 Formic acid is analytically challenging to measure due to its ‘stickiness’ in sample inlets and its
294 humidity/temperature dependent sensitivities in PTR-ToF^{34,53} and I⁻ CIMS^{43,48}. Figure 1 shows
295 the 1 Hz time series and cumulative mixing ratios of FA measured by PTR-ToF and I⁻ CIMS
296 during five plume transects (< 20 km downwind) of the Taylor Creek (TC) fire sampled during
297 WE-CAN (Research Flight #3). When corrected for inlet residence times, the two measurements
298 show good temporal agreement, capturing the real-time plume variability. However, the PTR-
299 ToF consistently measures $\sim 2 \times$ lower maximum FA concentrations than the I⁻ CIMS during the
300 plume transects likely representing sample retention in the inlet, a baseline offset due to
301 background correction differences, and/or calibration errors.

302



303

304 **Figure 1.** Time series of 1 Hz PTR-ToF and I CIMS formic acid mixing ratios (bottom panel)
 305 and cumulative mixing ratios for each plume through the following background period (top
 306 panel) during 5 plume transects made < 20 km downwind from the Taylor Creek Fire, OR during
 307 WE-CAN.

308

309 The TC fire was sampled shortly after injection into the free troposphere with little to no regional
 310 smoke impacts, resulting in clearly defined plume edges that can be seen in Figure 1 by the rapid
 311 FA enhancement upon entry into the smoke. However, when exiting the plumes, the PTR-ToF
 312 trace shows a distinct tail indicative of FA being initially retained in the inlet before flushing out
 313 in the 60–90 seconds after returning to background air. This is further illustrated by the upper
 314 panel in Figure 1, where the cumulative mixing ratios for each plume through the subsequent
 315 background sampling periods are shown for both instruments. For all plumes shown in Figure
 316 the I CIMS and PTR-ToF integrated FA mixing ratios agree within <50 % after accounting for
 317 residual FA in the inlet. This indicates that the two measurements agree within their stated
 318 uncertainty given sufficient time to recapture FA from the PTR-ToF inlet. However, Plumes 2
 319 and 3 also demonstrate how FA may wash out of the inlet and increase the signal in subsequent
 320 transects. Due to most other sampling periods having either more poorly defined plume edges,
 321 elevated background signals from regional smoke, and/or not having enough time between

322 consecutive transects, we are unable to accurately extend this analysis to other fires. It is likely
323 though that inlet retention decreases the maximum PTR-ToF measured FA in most plumes
324 sampled during WE-CAN.

325
326 The lack of a similar inlet artifact in the I⁻ CIMS measurement is likely explained by a few
327 characteristics. First, inlet sizes and materials differ slightly between the two instruments. The I⁻
328 CIMS inlet is significantly shorter than the one used by the PTR-ToF, resulting in a shorter
329 residence time in I⁻ CIMS (< 0.7 vs. 2 s). The I⁻ CIMS inlet was also comprised of only PTFE,
330 while the PTR-ToF used PFA and PEEK tubing. Second, the I⁻ CIMS fast zeroing strategy (seen
331 as the data gaps in the I⁻ CIMS trace in Figure 1) results in a FA background-subtracted signal
332 that minimizes the effects of adsorption and desorption from walls and surfaces in the
333 instrument.⁴⁵ Consequently, this points to the importance of the instrument's inlet configuration
334 and background correction procedures for the most accurate measurement of FA in environments
335 with rapid concentration changes.

336
337 Although inlet retention explains a large part of the disagreement of FA measured by the two
338 instruments while sampling smoke plumes with high, rapidly changing concentrations, the
339 average flight integrated I⁻ CIMS (120 ± 61 ppm) to PTR-ToF (66 ± 28 ppm) formic acid ratio of
340 2.1 and total least squares regression (TLS; slope = 2.06, $r^2 = 0.82$), indicates that the I⁻ CIMS
341 measured $\sim 2 \times$ more FA than the PTR-ToF across all research flights (Figure S3). Although the
342 exact reason for this disagreement is unknown, it likely stems from both a baseline offset and
343 calibration uncertainty. For example, the PTR-ToF inflight zeros may have contained residual
344 FA due to desorption from the instrument/inlet surfaces and/or incomplete oxidation in the
345 catalyst-generated zero air. Consequently, an excessive background signal was subtracted,
346 resulting in the mixing ratios being biased slightly low, especially when sampling relatively
347 clean air.

348
349 The FA sensitivity in I⁻ CIMS is also strongly dependent on IMR temperature,⁴⁸ which was not
350 directly controlled or logged during WE-CAN. The IMR used during WE-CAN⁴⁵ was different
351 than the IMR used in Robinson et al.,⁴⁸ with each also operated at different pressures (100 mbar
352 vs 40 mbar). Although variability in IMR temperature may influence the I⁻ CIMS FA sensitivity

353 during WE-CAN, instrument differences likely change the temperature dependence between
354 studies in ways that have not been tested. Consequently, the full extent of temperature effects on
355 the I CIMS sensitivity during WE-CAN is unknown and future work should focus on controlling
356 IMR temperature while further characterizing the sensitivity dependence on temperature under
357 different instrument conditions.

358
359 We repeat a similar analysis with FIREX-AQ FA measurements and find that in contrast to WE-
360 CAN, the PTR-ToF generally measured slightly lower FA mixing ratios than the I CIMS (TLS
361 slope = 0.87, $r^2 = 0.78$) for all FIREX-AQ data at altitudes below ~4.9 km, with the two agreeing
362 well within their stated instrument uncertainty. When compared between regions, the FIREX-
363 AQ-W FA measurements shows better agreement (slope = 0.89, $r^2 = 0.82$) than FIREX-AQ-SE
364 (slope = 0.69, $r^2 = 0.67$), possibly representing uncertainty in the instrument sensitivity due to the
365 higher humidity typical of the southeastern U.S. relative to the western U.S. (Figure S3).
366 Additionally, neither instrument shows significant inlet retention, with FA mixing ratios for both
367 instruments generally returning to background levels at the same rate after exiting plumes
368 (Figure S4).

369
370 The observed disagreement between the two instruments during WE-CAN is likely due to a
371 combination of factors including uncertainty in the FA sensitivity due to its humidity and
372 temperature dependence, potential instrument drift between the laboratory calibrations and field
373 measurements, inlet losses, and differences in background correction procedures. FIREX-AQ FA
374 measurements largely corrected for these issues by using a shorter PTR-ToF inlet along with
375 correcting for the I CIMS IMR temperature variations. Consequently, to improve future FA
376 measurements made by I CIMS and PTR-ToF special attention should be given to shortening
377 inlet residence times and minimizing sensitivity dependencies on temperature and humidity.

378
379 In this work, we primarily use I CIMS FA measurements for most analysis and discussion due to
380 its lower detection limits and lack of apparent inlet artifacts. This is likely an upper bound for
381 WE-CAN data and therefore we include PTR-ToF FA observations to further constrain the
382 measurement uncertainty where appropriate. We note that despite the high uncertainty in the FA

383 measurements (up to 100%), model underestimates discussed in Section 6 are much greater than
384 the measurement uncertainty.

385 **4 Emissions of formic and acetic acid from WE-CAN sampled fires**

386 Emission ratios (ERs) and emission factors (EFs) were calculated for 31 WE-CAN emission
387 transects of 24 individual fires as described in Permar et al.¹⁸ Here, emission transects are
388 defined as the nearest transect of a well-defined smoke plume that is traceable to a single
389 emission source sampled 27–130 minutes downwind from the fire, as calculated by wind speeds
390 measured aboard the C-130 and fire locations reported by the U.S. Forest Service.¹⁸ Although
391 these transects represent the freshest smoke sampled during the campaign, this is sufficient time
392 for substantial secondary formation to have occurred.^{19,46,68,69} Consequently, FA and AA ERs
393 and EFs during WE-CAN represent their combined production and loss before being sampled by
394 the research aircraft, which may be more appropriate for the spatial and temporal resolution of
395 many CTMs.⁷⁰ Normalized excess mixing ratios (NEMRs) were calculated using the background
396 corrected plume integrated mixing ratios of a VOC to CO (ppb VOC ppmco⁻¹) for each emission
397 and subsequent downwind plume transect. ERs were used to calculate EFs, expressed as grams
398 of VOC emitted per kilogram of burned fuel, using the carbon mass balance method^{23,71} with the
399 total emitted carbon as the sum of CO₂, CO, CH₄, organic carbon, black carbon, and 161
400 VOCs.¹⁸ Fuels burned during WE-CAN were primarily those characteristic of mixed conifer
401 forests.

402
403 Literature values were compiled from 16 different papers, reporting 330 FA and 289 AA ERs
404 and EFs.⁷² Approximately half of the EFs were also recorded and retrieved from the Smoke
405 Emissions Reference Application (SERA), which may include some additional values
406 recalculated to match their fuel types.⁷³ Average FA and AA ERs and EFs for the literature
407 described in this work are summarized in Table S1 and represent a variety of burned fuels. Pre
408 2007 FA data measured by Fourier transform infrared spectroscopy (FTIR) have also been
409 corrected by a factor of 2.1 following Yokelson et al.⁷⁴ Similar to vegetation classifications in
410 global BB emissions inventories, we broadly categorize these ERs and EFs as conifer forest (147
411 FA and 122 AA EFs), mixed hardwood forest (17, 23), shrubland (53, 38), grassland (36, 31),
412 crop residue (46, 47), and organic soil/peat (31, 28). Table S1 also includes modified combustion

413 efficiency (MCE) when available, instrumentation used, region of fuels burned, and whether the
414 data are from a laboratory or field study.^{19,20,23,25,26,34,75–78}

415
416 Figure 2 shows FA and AA ERs for each of the 24 fires sampled during WE-CAN (green
417 points), 16 fires sampled during FIREX-AQ, and literature values for all fuel types in our review
418 (box-and-whisker plots). During WE-CAN, the average formic acid ER calculated from I⁻ CIMS
419 data was found to be 9.5 ± 4.2 ppb ppm_{CO}⁻¹ (Table 1), which is 3.5 times higher than the
420 literature average of 2.7 ± 2.6 ppb ppm_{CO}⁻¹ calculated from 168 data points reported for 10 of the
421 16 studies in Table S1. We note that although FA ERs calculated from PTR-ToF measurements
422 (average 6.6 ± 2.5 ppb ppm_{CO}⁻¹) are slightly lower than those from I⁻ CIMS, both are generally
423 higher than the 75th percentile of literature values. Similarly, though FA ER during FIREX-AQ
424 (average 3.31 ± 2.0 ppb ppm_{CO}⁻¹) are lower than during WE-CAN, half are still above the 75th
425 percentile of the literature. Additionally, constraining ERs to only western U.S fuels has little
426 effect on this comparison as discussed in more detail below.

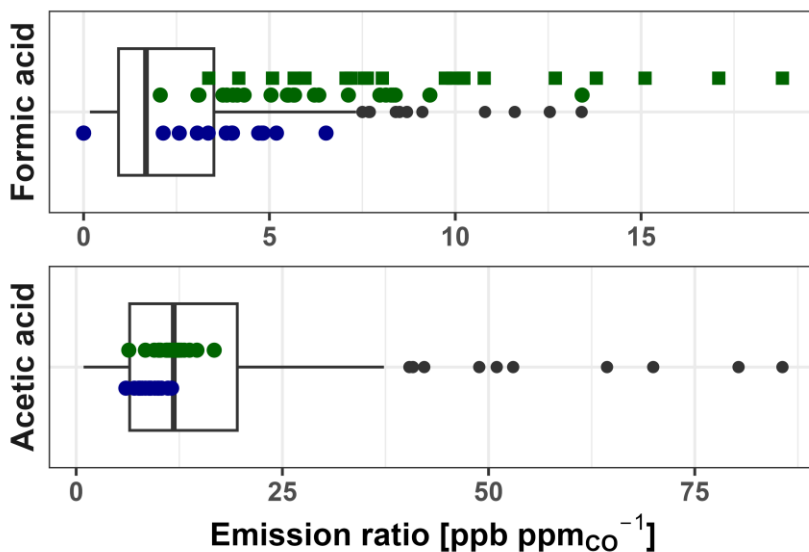
427
428 One possible explanation for the higher ERs observed during WE-CAN and FIREX-AQ is that a
429 significant amount of FA has been produced in the plumes prior to being intercepted by the C-
430 130 (Section 5). To approximate how much FA may have been formed before being sampled, we
431 estimate t_0 emission ratios from the least squares regression of WE-CAN NEMRs *vs.* physical
432 age for three of the five pseudo-Lagrangian sampled smoke plumes discussed in Section 5.
433 Assuming a constant production rate, projected FA NEMRs from I⁻ CIMS measurements at t_0
434 range from 5.7–7.4 ppb ppm_{CO}⁻¹, which is still approximately 2–3 times higher than the literature
435 average. Consequently, while many of the FA ERs measured during WE-CAN likely reflect
436 some plume aging (which, although hard to quantify, may also be the case in literature values),
437 near-field production alone is not enough to explain the disagreement. Given that WE-CAN ERs
438 calculated using both I⁻ CIMS (9.5 ppb ppm_{CO}⁻¹) and PTR-ToF (6.6 ppb ppm_{CO}⁻¹) measurements
439 agree within their stated uncertainty, it is likely that the ERs observed during WE-CAN generally
440 represent higher FA emissions from the wildfires sampled that season than the literature average
441 (Figure S6). As FIREX-AQ FA ERs are also generally higher than the literature, this may in part
442 reflect the bias of these two datasets towards sampling relatively large wildfires, which could
443 produce different FA emissions than laboratory burns and the smaller fires predominantly

444 represented in the literature. We recommend that future studies report their estimated aging when
445 reporting FA ERs.

446
447 In contrast, AA ERs measured during WE-CAN and FIREX-AQ mostly fall within the 25th–75th
448 percentiles of literature values (Figure 2 and Table 1), with good agreement between their
449 averages (WE-CAN 11.5 ± 2.1 ppb ppm_{CO}⁻¹, FIREX-AQ 8.9 ± 1.5 ppb ppm_{CO}⁻¹, literature $15.5 \pm$
450 14.2 ppb ppm_{CO}⁻¹).

451
452 Figure S5 shows that FA EFs follow the same trend as the ERs, with the WE-CAN average EF
453 of 1.5 ± 0.60 g kg⁻¹ (PTR-ToF = 0.96 ± 0.39 g kg⁻¹) and FIREX-AQ average EF of 0.6 ± 0.42 g
454 kg⁻¹ approximately 5 and 2 times higher than the literature average of 0.35 ± 0.48 g kg⁻¹
455 Similarly, both campaign AA EFs are within the 25th-75th percentile of literature values, with
456 good agreement between their averages (WE-CAN 2.4 ± 6.1 g kg⁻¹, FIREX-AQ 2.1 ± 6.3 g kg⁻¹,
457 literature 2.5 ± 2.6 g kg⁻¹).

458
459



460
461 **Figure 2:** Emission ratios of formic and acetic acid for literature values (box-and-whisker), WE-
462 CAN PTR-ToF observations (green points), I-CIMS FA (green squares), and FIREX-AQ PTR-
463 ToF (blue points). The box and whisker plots reported include literature ERs from all studies in
464 Table S1, representing a variety of fuels (204 data points for formic acid and 196 for acetic acid).

465 Boxes represent the 25th and 75th percentiles, with vertical lines as median, whiskers as $1.5 \times$ the
466 interquartile range, and black points as $> 1.5 \times$ interquartile range of literature values.

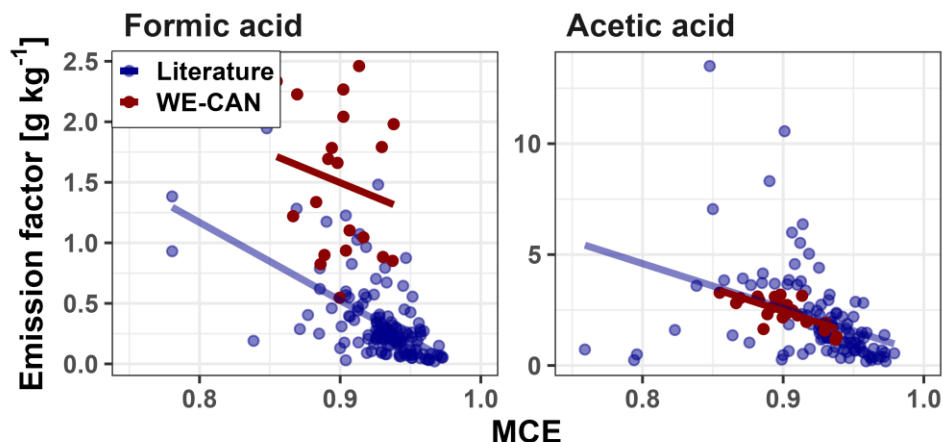
467
468

469 To examine if the observed organic acid emission variability is related to burning condition, we
470 compare the derived EFs from WE-CAN and literature coniferous forests to the modified
471 combustion efficiency, which is a simple proxy used to describe the degree of flaming versus
472 smoldering combustion in a fire. MCE is defined as,

$$473 \quad MCE = \frac{\Delta CO_2}{\Delta CO_2 + \Delta CO} \quad (1)$$

474 where ΔCO_2 and ΔCO are the excess CO_2 and CO mixing ratios. An MCE near 1 corresponds to
475 pure flaming combustion, while MCEs of 0.65–0.85 represents pure smoldering.⁷⁹ During WE-
476 CAN, MCEs ranged between 0.86–0.94, while those for mixed conifer forests in our literature
477 review have a larger range of 0.76–0.98. We note that MCEs span 0.68–0.99 when including all
478 fuel types in our literature review, with most MCEs < 0.84 corresponding to combustion of peat
479 and organic soils. Figure 3 shows FA and AA EFs vs MCE for both WE-CAN sampled fires and
480 coniferous forest literature values. The WE-CAN and literature EFs for FA have only a weak
481 negative dependence on MCE, with slopes of -4.8 ($r^2 = 0.03$) and -6.4 ($r^2 = 0.35$) respectively.
482 Using PTR-ToF FA data makes little difference, with the WE-CAN $r^2 = 0.05$. AA EFs have a
483 stronger negative correlation with MCE during WE-CAN (slope -20.7, $r^2 = 0.52$) and for
484 literature values (slope = -20.2, $r^2 = 0.14$). Expanding this analysis to include all fuel types in our
485 literature review results in a lower slope and r^2 for the literature FA (-3.0, 0.071) and a larger
486 slope and r^2 for AA (-27.3, 0.26). The poor correlation of FA EFs with MCE suggests that its
487 emissions variability is driven by factors other than combustion efficiency. Conversely, AA
488 emissions likely have some MCE dependence that should be accounted for when reporting and
489 using EFs.

490



491

492 **Figure 3:** Correlations of FA (left) and AA (right) EFs versus MCE for both WE-CAN (red
 493 points) and literature reported coniferous forest values (blue points). The least squares regression
 494 for each group is shown in corresponding colors. For FA, the line of best fit for WE-CAN data is
 495 $y = -4.8x + 5.8$ ($r^2 = 0.03$) and $y = -6.4x + 6.3$ ($r^2 = 0.35$) for literature values. For AA, the line of
 496 best fit for WE-CAN data is $y = -20.7x + 21.1$ ($r^2 = 0.52$) and $y = -20.2x + 20.8$ ($r^2 = 0.14$) for
 497 literature values. Detailed statistics including PTR-ToF FA are shown in Table 1.

498

499

500 To determine if the type of fuel burned influenced FA or AA emissions, we compare WE-CAN
 501 and literature EFs between the six fuel categories described above. For each organic acid we use
 502 a Tukey's range test to evaluate if the 95 % confidence interval (CI) of emission factors for each
 503 fuel type overlap. For FA, the Tukey range test p-values are > 0.05 for comparisons between all
 504 fuel types except with shrubland, indicating an overlap in the 95 % CI for most fuels. This
 505 suggests that FA EFs for shrubland, mainly consisting of chaparral vegetation types in our
 506 literature review, have statistically significant differences from the other 5 fuel categories.
 507 Alternatively, no statistical difference was found between any of the other categories. Coupled
 508 with the lack of correlation with MCE, this suggests that a single FA ER of 3.5 ± 3.4 ppb ppm_{CO}⁻¹
 509 and EF of 0.42 ± 0.56 g kg⁻¹ (average of WE-CAN, FIREX-AQ, and literature values $\pm 1\sigma$,
 510 Table 1) best describe most BB emissions, though a fuel-specific EF for shrubland fuels ($0.11 \pm$
 511 0.09 g kg⁻¹) may be more accurate.

512

513 AA EFs between coniferous forests, mixed hardwood forests, shrubland, and grassland similarly
 514 show no statistically significant fuel related difference, and an average ER of 14.5 ± 12.8 ppb
 515 ppm_{CO}⁻¹ and EF of 2.0 ± 1.9 g kg⁻¹ may best describe most fuel types. However, organic soil/peat

516 and crop residue both have p-values < 0.05 when compared to the other four fuels, suggesting
 517 that MCE and fuel dependent EFs may be needed to best describe AA EFs. Given that AA shows
 518 some dependence on MCE, it is possible that the differences between crop residue and organic
 519 soil/peat EFs compared to EFs for the other fuel categories is in part due to combustion
 520 efficiency. For example, organic soil/peat combustion is generally dominated by smoldering
 521 (MCE = 0.68–0.92 in this work), which would result in higher EFs (Figure 3). Box plots of FA
 522 and AA EFs for each fuel category are shown in Figure S6.

523

524 **Table 1:** Emission factors (g kg^{-1}) and emission ratios ($\text{ppb ppm}_{\text{CO}}^{-1}$) for formic and acetic acid
 525 reported in this work and in the literature. Note that the recommended average for FA is
 526 calculated from WE-CAN I⁻ CIMS, FIREX-AQ PTR-ToF, and all literature values. The
 527 recommended average for AA are calculated from WE-CAN PTR-ToF, FIREX-AQ PTR-ToF,
 528 and all literature values excluding crop residue and organic soil/peat.

529

| | WE-CAN | FIREX-AQ | Literature average | Recommended Average | |
|--------------------|-----------------------------|-----------------------------------|-----------------------------|-------------------------------------|---|
| Formic acid | ER $\pm 1\sigma$ (range) | 9.5 \pm 4.2 (3.4–18.8) | 3.3 \pm 2.0 (0–6.5) | 2.7 \pm 2.6 (0.17–13.4) | 3.5 \pm 3.4 |
| | EF $\pm 1\sigma$ (range) | 1.5 \pm 0.60 (0.55–2.5) | 0.60 \pm 0.42 (0–1.6) | 0.35 \pm 0.48 (0.002–4.2) | 0.42 \pm 0.56 |
| | n. obs. | 20 | 16 | 168 ERs, 330 EFs | 204, 366 |
| | Eq. with MCE | $y = -4.8x + 5.8$ $r^2 = 0.03$ | | $y = -6.4x + 6.3$ $r^2 = 0.35$ | $y = -9.7x + 9.4$ $r^2 = 0.31$ |
| Acetic acid | ER $\pm 1\sigma$ (range) | 11.5 \pm 2.1 (6.4–16.7) | 8.9 \pm 1.5 (6.0–11.7) | 15.5 \pm 14.2 (0.9–85.6) | 14.5 \pm 12.8 |
| | EF $\pm 1\sigma$ (range) | 2.4 \pm 6.1 (1.2–3.3) | 2.1 \pm 0.63 (1.1–3.4) | 2.5 \pm 2.6 (0.14–14.0) | 2.0 \pm 1.9 |
| | n. obs. | 24 | 16 | 156 ERs, 289 EFs | 196, 254 |
| | Eq. with MCE | $y = -20.7x + 21$ $r^2 = 0.52$ | | $y = -20.2x + 20.8$ $r^2 = 0.14$ | $y = -19.9x + 20.5$ $r^2 = 0.15$ |

530

531 **5 Near-field acid production during WE-CAN**

532 FA and AA concentrations varied widely during WE-CAN with maximum mixing ratios of 98
 533 ppb and 89 ppb, respectively. The highest FA NEMR of 71 ppb $\text{ppm}_{\text{CO}}^{-1}$ was observed in smoke
 534 aged ~13 hours. ERs were not measured for this fire; however, this is $\sim 7 \times$ higher than campaign

535 average ER (9.5 ± 4.2 ppb ppm_{CO}⁻¹), and $4 \times$ higher than the maximum ER (18.8 ppb ppm_{CO}⁻¹).
536 This suggests a maximum FA production rate of 4.0–4.7 ppb ppm_{CO}⁻¹ h⁻¹ in aged smoke sampled
537 during WE-CAN. This NEMR is approximately half of the maximum observed during ATom in
538 smoke sampled off the African coast estimated to have been aged 1–10 days (140 ppb ppm_{CO}⁻¹),
539 though this latter value is similar to many other plumes intercepted during that campaign.¹⁷

540
541 Figure 4 shows FA and AA NEMRs as a function of smoke plume age for 5 fires with more than
542 10 plume transects sampled in a pseudo-Lagrangian fashion during WE-CAN, while NEMRs for
543 all sampled plumes are shown in Figure S7 for reference. In the first 8 hours of plume aging FA
544 is rapidly produced at an average rate of 2.7 ppb ppm_{CO}⁻¹ h⁻¹. This is in good agreement with FA
545 production seen in other studies including 2.6–3.3 ppb ppm_{CO}⁻¹ h⁻¹ in smoke from Alaskan boreal
546 forest fires,²⁰ 1.6 ppb ppm_{CO}⁻¹ h⁻¹ from BB in the Yucatan, Mexico,²² and 0.9 ppb ppm_{CO}⁻¹ h⁻¹ in
547 chaparral fires in California.¹⁹ We hypothesize that the rapid FA production observed during
548 WE-CAN is at least in part responsible for the higher FA EFs and ERs discussed in Section 3.

549
550 During WE-CAN, AA NEMRs remain relatively constant in the first 8 hours of plume aging,
551 increasing by a statistically insignificant 0.3 ppb ppm_{CO}⁻¹ h⁻¹ ($p = 0.13$, $r^2 = 0.03$, Figure 4).
552 Additionally, the maximum AA NEMR was observed to be 17 ppb ppm_{CO}⁻¹ in the same ~13 hour
553 aged plume discussed above, which is within 3σ of the campaign average ER. The extent that
554 AA is produced in BB plumes is not well understood. For example, no net AA production has
555 similarly been observed in smoke aged 1.4 hour over the Mexican Yucatán Peninsula²² nor
556 inferred in BB plumes measured across Alaska and western Canada.⁸⁰ However, multiple other
557 studies have observed rapid AA production in the first few hours of plume aging including: 2.3
558 ppb ppm_{CO}⁻¹ h⁻¹ in smoke from a Californian chaparral fire aged 4.5 hours,¹⁹ 1.5 ppb ppm_{CO}⁻¹ h⁻¹
559 in 1 hour aged smoke from southeast U.S. prescribed agricultural burning,³⁴ 1.5–2.0 ppb ppm_{CO}⁻¹
560 h⁻¹ in smoke aged < 1 hour from African Savannah fires,²⁶ and 7.2 ppb ppm_{CO}⁻¹ h⁻¹ in smoke aged
561 1 hour from Alaskan boreal forest fires.²⁰ Future work is needed to better characterize AA
562 production, especially in smoke that has aged more than half a day.

563
564 One potential explanation for the lack of observed AA production during WE-CAN is that the
565 removal of glycolaldehyde offsets the formation of AA. This is possible because AA measured

566 by PTR-ToF may be ~30 % glycolaldehyde in fresh emissions,^{25,63} both species have similar
567 sensitivities in PTR-MS,⁵³ and glycolaldehyde is ~20 × more reactive than AA with OH (k_{OH}
568 $1.1 \times 10^{-11} \text{ cm}^3 \text{ molecule}^{-1} \text{ s}^{-1}$ vs. $7.4 \times 10^{-13} \text{ cm}^3 \text{ molecule}^{-1} \text{ s}^{-1}$; NIST chemical kinetics database
569 average). Additionally, of the studies that observed AA production listed above, only Muller et
570 al.³⁴ used a PTR-ToF while the others used FTIR, which does not have isomeric interferences for
571 AA. To test this hypothesis, we attribute only 66 % of the PTR-ToF m/z 61 to AA to calculate a
572 corrected campaign average ER of 7.6 ppb ppm_{CO}⁻¹. Assuming there is negligible glycolaldehyde
573 formation downwind, such that the PTR-ToF is only measuring AA in aged smoke, the
574 maximum AA production rate over ~13 hours of plume aging would be 0.7 ppb ppm_{CO}⁻¹ h⁻¹.
575 Although this production rate is still lower than in the literature, the 30 % reduction in the
576 campaign average AA ER brings it outside of the observed NEMR variance for most aged smoke
577 samples. This suggests that AA production could be statistically significant if these assumptions
578 are true, and more detailed characterization of the glycolaldehyde interference in aged smoke is
579 needed.

580
581 It is also possible that most of the AA formation happens in the first hours of plume aging, which
582 is then averaged out in our analysis of plumes that are aged 8 hours during WE-CAN. For
583 example, in one plume, Goode et al.²⁰ observed an AA increase of 11 ppb ppm_{CO}⁻¹ in the first 1.5
584 hours of plume aging followed by no net production relative to emissions in 2.8 hour old smoke.
585 However, limiting WE-CAN observations to those with <2 hours aging in Figure 4 still results in
586 a non-statistically significant NEMR-vs-age slope of 0.23 ppb ppm_{CO}⁻¹ h⁻¹ ($p = 0.80$, $r^2 = 0.002$).
587 Similarly, if each of the 5 fires in Figure 4 are treated individually, only two have statistically
588 significant correlations ($p = 0.02$) with plume age, both with negative slopes (-0.2 and -0.3 ppb
589 ppm_{CO}⁻¹ h⁻¹). Given the relatively long atmospheric lifetime of AA (~2-3 days),^{8,38} it is unlikely
590 that a significant amount was removed from the plume in the 8 hours of aging shown here.
591 Consequently, these results suggest that most of the observed AA in the near-field during WE-
592 CAN is from primary emissions, though photochemical production may still be an important
593 source in some fires and over longer plume aging times which should be investigated further.

594
595 Previous work has used the Framework for 0-D modeling (F0AM)⁸¹ to simulate the Taylor Creek
596 (TC) fire sampled during WE-CAN due to it being a well isolated plume with pseudo-

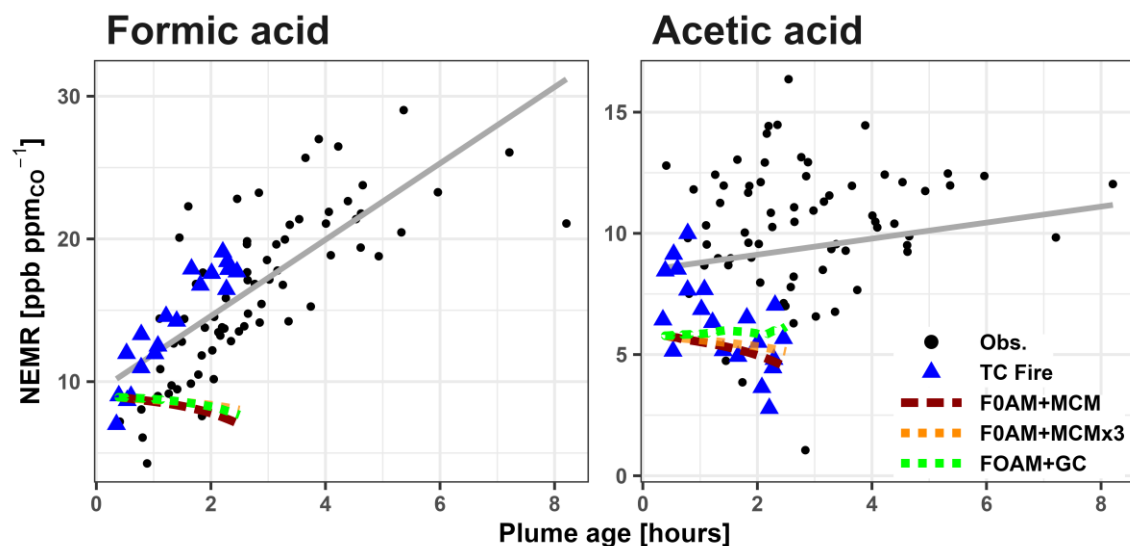
597 Lagrangian samples performed just after injection into the free troposphere.^{24,46,49,82–85} Here, we
598 use the same F0AM model run as originally described in Peng et al.⁸⁵ with updated VOC
599 emissions per Permar et al.²⁴ Briefly, F0AM was initialized using 49 VOCs, plus NO, NO₂,
600 HONO, O₃, and CO (Table S2). For VOCs measured by PTR-ToF, potential interfering isomers,
601 including glycolaldehyde, were removed so that the model was initialized based on the
602 proportion of the mass attributed only to the given species following Koss et al.²⁵ Physical
603 parameters such as photolysis frequencies, temperature, and pressure were constrained to
604 measured values at each model step with a dilution correction factor based on CO observations.
605 Model chemistry was simulated using the explicit Master Chemical Mechanism (F0AM+MCM)
606 including recently developed furans and phenolic chemistry,^{86,87} with an additional sensitivity
607 test run using $3 \times$ VOC initial values for all gases except FA and AA (F0AM+MCM \times 3). We also
608 run the same box model driven with the GEOS-Chem chemical mechanisms (F0AM+GC) to test
609 if recent updates by Chen et al.¹⁷ significantly impact the modeled FA production in fresh smoke.

610
611 Figure 4 shows that neither F0AM+MCM, F0AM+MCM \times 3, nor F0AM+GC can reproduce the
612 rapid FA formation observed in the TC plume, with modeled FA instead decreasing slightly with
613 plume age. The MCM predicted loss rate for FA in the base run to be ~ 0.3 ppb h⁻¹ by reaction
614 with OH, while there is minimal production (~ 0.01 ppb h⁻¹) from C₄H₆O₃ and CH₂OO Criegee
615 intermediates. Coupled with the MCM being insensitive to increased initial values, this
616 represents more FA being removed in the model than is being produced and indicates that both
617 the MCM and GC are missing a substantial amount of secondary FA production in BB smoke.

618
619 The total emitted VOC carbon during WE-CAN averaged 367.3 ± 29.6 ppb_C ppm_{CO}⁻¹.¹⁸ As the
620 average FA enhancement shown in Figure 4 is 21 ppb ppm_{CO}⁻¹, approximately 5.7 % of the VOC
621 carbon oxidation would need to go to FA to explain the observed production. Additionally, the
622 maximum observed FA NEMR of 71 ppb ppm_{CO}⁻¹ after ~ 13 hours of plume aging represents a
623 61 ppb ppm_{CO}⁻¹ enhancement relative to the campaign average ER, indicating that up to 17 % of
624 the total emitted carbon could be converted to FA within half a day.

625
626 AA NEMRs in the TC plume are highly variable, likely representing changes in fire emissions or
627 sampling different parts of the plume. Figure 4 shows that F0AM+MCM and F0AM+GC

628 generally have good agreement with the observed AA NEMRs. Similar to FA, AA is also mainly
 629 lost in the MCM through reaction with OH at $\sim 0.4 \text{ ppb h}^{-1}$, with negligible production (< 0.01
 630 ppb h^{-1}) from CH_3CHOO Criegee intermediates and $\text{CH}_3\text{C(O)O}_2$ peroxy acetyl radicals.
 631



632

633 **Figure 4:** NEMRs of FA and AA for 5 research flights with more than 10 pseudo-Lagrangian
 634 transects. Blue triangles highlight plume transects of the Taylor Creek (TC) fire and correspond
 635 to the red dashed F0AM+MCM, orange F0AM+MCM $\times 3$, and green F0AM-GC predicted
 636 NEMRs for the same fire. Black points correspond to the other 4 fires. Least squares regression
 637 lines for the aggregated data are shown in gray. During the first 8 hours of plume aging FA
 638 NEMR increased on average $2.7 \text{ ppb ppmCO}^{-1}$ per hour ($r^2 = 0.58$, intercept = $9.3 \text{ ppb ppmCO}^{-1}$),
 639 while AA has a statistically insignificant increase of $0.3 \text{ ppb ppmCO}^{-1}$ per hour ($r^2 = 0.03$,
 640 intercept = $8.4 \text{ ppb ppmCO}^{-1}$).
 641

642

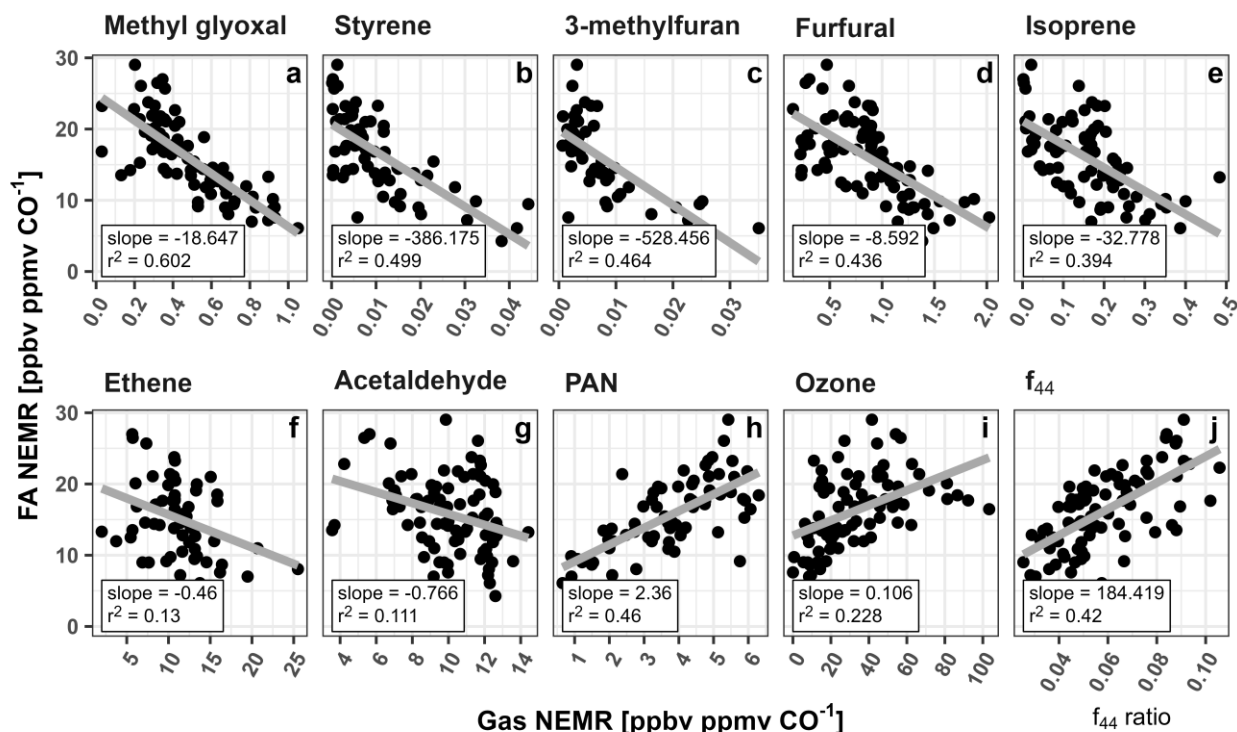
642 A current lack of understanding of the major FA and AA precursors is one of the largest hurdles
 643 to accurately modeling their evolution in smoke. To evaluate potential VOC precursors, NEMRs
 644 for both acids measured in the same 5 wildfires as described above were compared to NEMRs of
 645 152 VOCs measured during WE-CAN using least squares regression. FA was found to have
 646 statistically significant negative correlations ($p\text{-value} < 0.05$, $r^2 > 0.10$) with 94 VOCs. Over the
 647 8 hours of plume aging the oxidation of these 94 species collectively accounts for 127 ppbc
 648 ppmCO^{-1} that is reacted away. This indicates that those species lose $6 \times$ more carbon than is
 649 needed to account for the observed FA production, though the exact chemical pathways are often
 650 unknown. For example, $\text{C}_3\text{H}_4\text{O}_2$ (methyl glyoxal + acrylic acid), styrene, and furanoid
 651 compounds such as 3-methylfuran and furfural are among the species with strongest correlations

652 to FA in fresh smoke during WE-CAN (Figure 5; $r^2 > 0.40$). However, the MCM and recent
653 chemical mechanism developments do not show any chemical production of FA from these
654 compounds.^{86,88,89}

655
656 Figure 5 similarly shows that FA is well correlated ($r^2 > 0.4$) with isoprene, ethene, and
657 acetaldehyde, consistent with the current understanding of these species being known FA
658 precursors. Additionally, FA was found to have a strong correlation with peroxyacetyl nitrate
659 (PAN; $r^2 = 0.46$) and a modest correlation with ozone ($r^2 = 0.23$), further indicating that FA
660 production follows the overall plume gas phase oxidization. While the correlations of FA
661 NEMRs with the VOCs in Figure 5 do not directly indicate that they are FA precursors in smoke
662 plumes, when coupled with FA being well correlated to PAN, ozone, and 94 different VOCs, they
663 do demonstrate that FA is likely being produced through the oxidation of many different species,
664 most of which are currently not well studied in the literature.

665
666 Heterogenous formation is also likely to be an important FA source in smoke via a multiphase
667 pathway where methanediol (HOCH_2OH) is off gassed from aerosols and is rapidly oxidized by
668 OH to form HCOOH .^{32,33} The WE-CAN dataset does not have sufficient data to fully examine
669 how this pathway may contribute to the FA production observed during the campaign. Instead,
670 we explore whether the FA NEMRs show dependence on OA aging during WE-CAN in Figure
671 5j by comparing FA NEMRs with the OA oxidation marker f_{44} .^{50,51} f_{44} is the fractional
672 component of OA attributed to the CO_2^+ ion which is ascribed to fragments of acids or acid-
673 derived species.⁹⁰ Consequently, f_{44} is generally well correlated with the OA elemental O:C
674 ratio,⁹¹ where both increase as the bulk aerosol becomes more oxidized. During WE-CAN f_{44}
675 was found to increase with smoke plume age, while the dilution-adjusted OA mass generally
676 remained unchanged over ~8 hours of plume aging.⁴⁹ Figure 5j shows that FA NEMRs are
677 positively correlated with f_{44} ($r^2 = 0.42$) as well as with the OA O:C ratio ($r^2 = 0.32$, not shown).
678 This suggests that FA production follows the bulk aerosol oxidation during WE-CAN.
679 Additionally, the increasing OA oxidation with the constant downwind dilution-adjusted OA
680 mass reported by Garofalo et al.⁴⁹ requires a balance between evaporation and condensation of
681 semivolatile species. This indicates that FA could be formed as part of this OA mass balance and

682 more detailed laboratory and field studies are needed to better understand this potentially
 683 significant FA formation pathway in BB smoke.
 684



685
 686 **Figure 5:** FA NEMRs compared to various gas phase species NEMRs and aerosol f_{44} ratios
 687 measured in 5 smoke plumes with more than 10 pseudo-Lagrangian plume transects. Slope and
 688 r^2 for the least squares regression of each species are shown at the bottom of each panel, while
 689 the gray lines represent the best fit. Panels a, b, and c show the three VOCs with the strongest
 690 correlation to FA. Panels d and e show two of the largest OH radical sinks (ranked by OH
 691 reactivity from individual VOC)²⁴ that are highly correlated with FA in wildfire emissions.
 692 Panels f, and g show known FA precursors, while quantities plotted in h, i and j are
 693 representative of the overall plume oxidation. Note, methyl glyoxal is measured with acrylic acid
 694 ($C_3H_4O_2$). PAN = peroxyacetyl nitrate. f_{44} = ratio of m/z 44 to the total signal in the aerosol
 695 component spectrum with higher ratios indicating more aged organic aerosol and higher O:C.
 696

697 Similar analysis with AA is shown in Figure S8, with AA NEMRs plotted against a similar
 698 grouping of gases as in Figure 5. The three species with the strongest correlation against AA are
 699 shown in Figure S8a, b and c: $C_3H_6O_2$ (hydroxyacetone + methyl acetate + ethyl formate; $r^2 =$
 700 0.62), $C_5H_8O_3$ (5-hydroxymethyl tetrahydro 2-furanone; $r^2 = 0.48$), and methyl propionate ($r^2 =$
 701 0.45). Like AA, NEMRs for these three species are not well correlated with the physical plume
 702 age. Figure S8 also shows that AA has only modest correlation with the reactive VOCs furfural

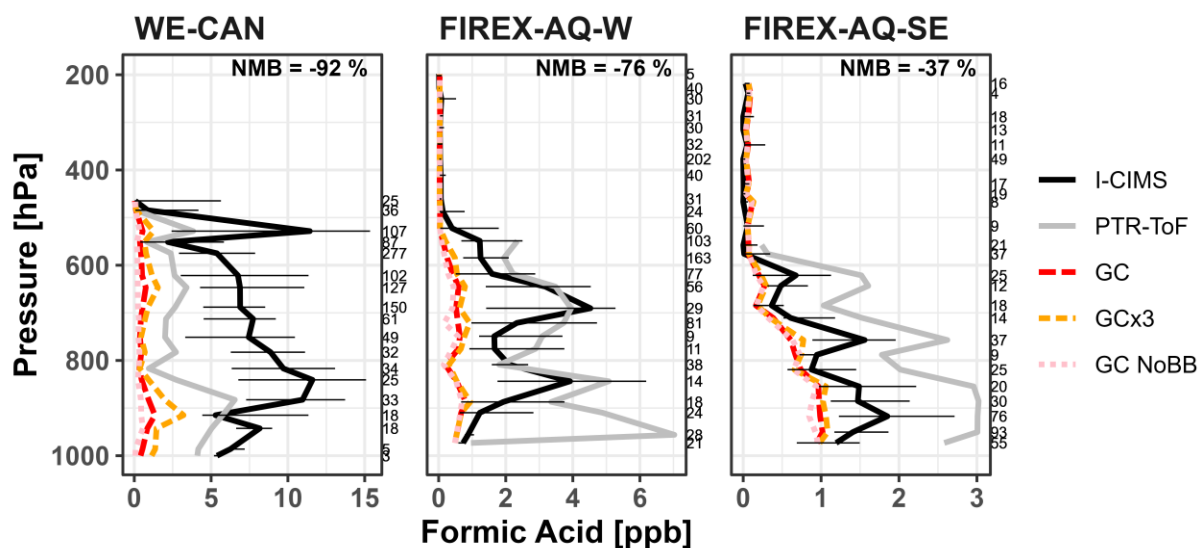
703 and isoprene as well as with acetaldehyde and ozone ($r^2 = 0.14\text{--}0.32$) but is poorly correlated
704 with ethene and PAN ($r^2 < 0.1$). The fact that a) AA is most strongly correlated with other VOCs
705 whose NEMRs remain mostly unchanged with plume age and b) has poor negative correlations
706 with the plume oxidation indicators such as PAN, ozone, and f_{44} , further supports the observation
707 that little AA is produced and instead is mainly from primary emissions in the WE-CAN sample
708 wildfire plumes.

709 **6 GEOS-Chem representation of FA and AA during WE-CAN and FIREX-AQ**

710 Global chemical transport models typically have difficulty simulating formic and acetic acid
711 mixing ratios, particularly in the presence of BB smoke. Section 5 suggests that the GEOS-Chem
712 chemistry underestimates a significant amount of secondary production of FA in fresh smoke.
713 Here we investigate how the GEOS-Chem CTM, with the most recent updates for FA
714 implemented by Chen et al.¹⁷ (Section 2.3), represents FA and AA in different environments
715 sampled during the WE-CAN, FIREX-AQ-W, and FIREX-AQ-SE. All WE-CAN and FIREX-
716 AQ measurements have also been averaged to 5 minutes to match the model resolution. GEOS-
717 Chem was sampled along the plane flight tracks at the time of each corresponding research
718 flight.

719
720 Figure 6 shows that GEOS-Chem generally underestimates the vertical distribution of FA
721 observed during WE-CAN (-92 %; normalized mean bias to I⁻ CIMS, NMB) and in the middle to
722 lower troposphere (>450 hPa or below ~7.2 km above sea level) during FIREX-AQ-W (-76 %
723 NMB) and FIREX-AQ-SE (-37 %). This corresponds to the model underestimating the average
724 measured FA by nearly a factor of 13 during the WE-CAN deployment, while also
725 underestimating FA by a factor of 4 and 2 in the lower altitude FIREX-AQ-W and FIREX-AQ-
726 SE samples. However, GEOS-Chem does significantly better simulating FA in the middle to
727 upper troposphere (<450 hPa; -27 % NMB in FIREX-AQ-W), consistent with findings by Chen
728 et al.¹⁷ Interestingly, GEOS-Chem overestimates FA mixing ratios compared to I⁻ CIMS
729 measurements at higher altitudes (< 450 hPa) in the southeastern U.S. (213 %), though the
730 measured FA is reaching the stated I⁻ CIMS detection limit (~30 ppt). Figure S9 shows a similar
731 underestimation for acetic acid mixing ratios with NMB ranging -92 % to -99 % in both high and
732 low altitude WE-CAN and FIREX-AQ-W samples, and slightly better agreement (-80 %) with

733 lower altitude FIREX-AQ-SE periods. We note that this significant underestimate of FA by
 734 GEOS-Chem holds true regardless of the high uncertainty in FA measured during the WE-CAN
 735 deployment as the difference between the modeled and measured values is much greater than the
 736 instrument uncertainty.
 737



738
 739 **Figure 6.** Vertical profiles of the median formic acid mixing ratios measured during the full WE-
 740 CAN and FIREX-AQ field campaigns, binned at every 33 hPa. Black and gray lines correspond
 741 to the measurements made by I-CIMS and PTR-ToF, with error bars representing the 25th and
 742 75th percentile of I-CIMS measurements at each pressure bin. Red dashed lines correspond to
 743 GEOS-Chem with GFAS BB emissions (GC), orange dashed lines represent GEOS-Chem with 3
 744 × GFAS BB emissions (GC×3), and the pink dotted lines show GEOS-Chem with BB emissions
 745 turned off (GC NoBB). The number of samples in each pressure bin are shown on the right of the
 746 plots, while the normalized mean bias (NMB) to the I-CIMS measurement for lower altitude
 747 observations (> 450 hPa) are shown at the top.
 748

749 There are a few possible explanations for why GEOS-Chem underestimates FA and AA during
 750 the two campaigns, including: incorrect or missing emissions, sampling bias, and/or missing
 751 secondary chemistry from BB (Section 5) and biogenic precursors. Recent model developments
 752 have improved the GEOS-Chem representation of the free troposphere,¹⁷ chemistry, and
 753 biogenic sources.⁷ Subsequently, we hypothesize that missing secondary production from BB
 754 and western U.S. specific biogenic precursors are likely key reasons for GEOS-Chem
 755 underestimating FA mixing ratios during WE-CAN and FIREX-AQ-W. The exact reason for the
 756 underestimation of AA mixing ratios is uncertain, though we speculate it may in part be due to

757 the model sink being too large³⁸ and/or secondary production in BB smoke aged over greater
758 processing times than discussed in Section 5 (i.e., > 8 hours).

759

760 **Model BB emissions and sampling bias**

761 Recent work has shown that commonly used global emission inventories, including GFAS,
762 GFED4, QFED, and FINNv1.5, underestimate BB emissions by a factor of three or more in the
763 western U.S. when compared to aircraft and ground-based measurements.^{41,92} Jin et al.⁴¹
764 attributes this mostly to the significant underestimation of the dry biomass burned in the BB
765 emission inventories. To explore if underestimated BB emissions can explain the low FA and
766 AA model bias, GEOS-Chem was also initiated with $3 \times$ GFAS BB emissions as a sensitivity
767 test, in which the BB VOC and CO emissions are tripled from the base run. Figure S10 shows
768 that GEOS-Chem with base GFAS emissions underestimate CO during WE-CAN, FIREX-AQ-
769 W, and FIREX-AQ-SE. Model representation in the western U.S. is improved by the $3 \times$ GFAS
770 model run, in good agreement with Jin et al.⁴¹ Similarly, though benzene and acetone are better
771 represented by the base model in this work, the $3 \times$ GFAS emission simulation further improves
772 their model agreement. Despite this, Figures 6 and S9 show that increasing BB emissions by a
773 factor of 3 only slightly increases the model FA and AA mixing ratios, decreasing the NMB by
774 $\sim 5\%$ in all cases. Given 1) that tripling BB emissions has minimal impact on the modeled FA or
775 AA, 2) that the GFAS inventory is not missing the location/timing of the fires sampled during
776 both campaigns,⁴¹ and 3) that FA and AA BB emissions were implemented per observed ERs,⁴¹
777 underestimation of primary BB emissions of either acid or their known precursors in GEOS-
778 Chem alone cannot account for the low model bias. This reflects that the contribution of primary
779 BB emissions to ambient FA during WE-CAN and FIREX-AQ in the western US is small.
780 Additionally, the $3 \times$ GFAS run also increases emissions for all BB implemented species,²⁴ thus
781 pointing to missing secondary formation pathways from either implemented and/or unknown
782 precursors in the model (see Section 5). Given the lack of evidence for near-field AA production
783 during WE-CAN, the model being largely insensitive to a 3-fold increase in AA emissions
784 suggests that AA production in BB plumes aged greater than the 8 hours observed during WE-
785 CAN may still be significant and/or the overall model sink is too large.

786

787 The WE-CAN and FIREX-AQ aircraft campaigns were focused on sampling and tracking BB
788 smoke whenever possible. As GEOS-Chem was run at $0.25^\circ \times 0.3125^\circ$ (~25 km) resolution, the
789 low model bias may in part also reflect the dilution of narrow smoke plumes over the model grid.
790 Though some error is inherent in the model comparisons due to this sampling bias, using GEOS-
791 Chem run with the same WE-CAN and FIREX-AQ datasets, Jin et al.⁴¹ demonstrated that the
792 model also had difficulty simulating smoke impacts at longer term ground measurement sites
793 across the western U.S. This is indicative that the low model biases cannot be explained by the
794 model resolution alone. Similarly, Jin et al.⁴¹ showed that fire detection products across emission
795 inventories did well capturing the large fires sampled during WE-CAN and that GEOS-Chem is
796 fairly insensitive to plume injection heights for the averaged WE-CAN campaign, likely due to
797 efficient vertical mixing during the summer months.^{93,94} However, because of these issues when
798 comparing fire plumes sampled by aircraft to global CTMs, the GEOS-Chem evaluation here
799 further focuses on the campaign averages across two different years, in smoke impacted, no/low
800 smoke, and clean free troposphere environments.

801

802 **Representation in different environments**

803 To investigate potential model deficiencies over broad regions, we further examine the model
804 performance in different environments sampled during the campaigns as described in our
805 previous work.²⁴ Here, smoke-impacted sampling periods for both campaigns are defined as
806 those with hydrogen cyanide (HCN) > 250 ppt and acetonitrile (CH₃CN) > 200 ppt, while
807 periods below this threshold are discussed as low/no-smoke. However, due to widespread
808 regional smoke during the fire season, the low/no-smoke samples likely still represent some BB
809 influence. In addition to this coarse filter, clean free troposphere samples were also defined for
810 both campaigns based on HCN < 250 ppt, CH₃CN < 150 ppt, and pressure < 624 hPa (~4 km
811 above sea level, representing the maximum boundary layer height as determined from vertical
812 temperature profiles).

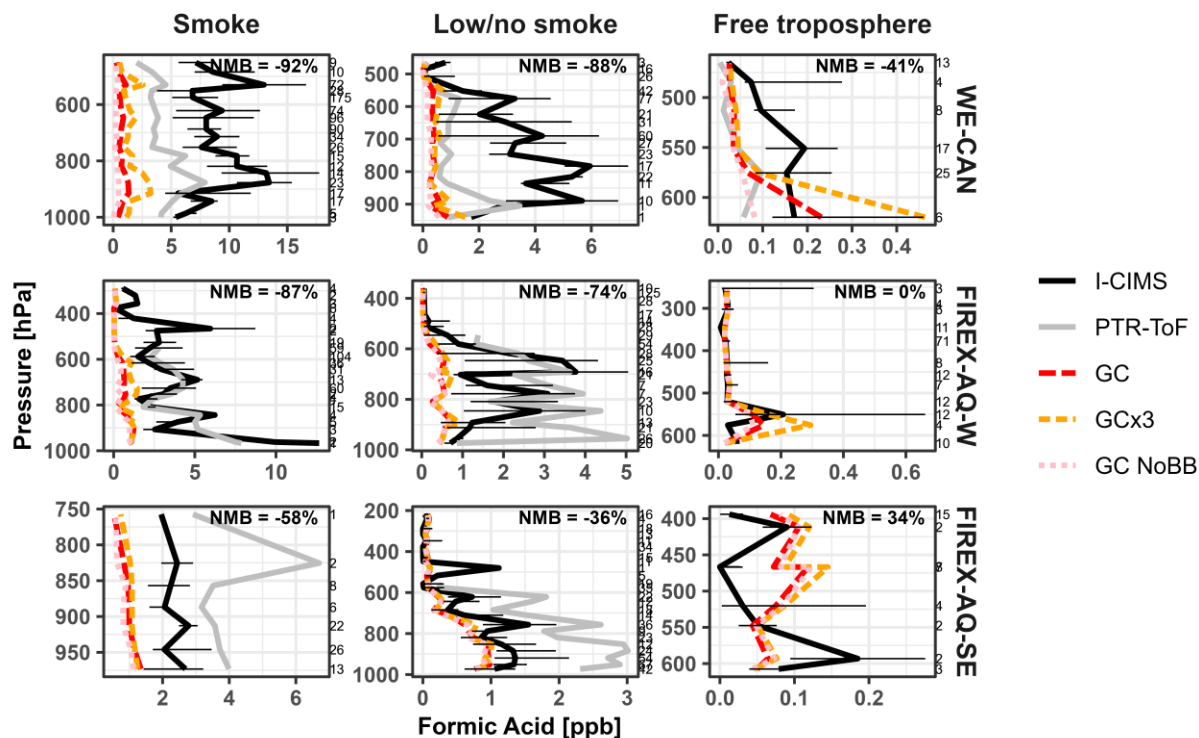
813

814 Figure 7 shows the vertical profiles for the median observed and modeled FA in the three
815 different environments. We find GEOS-Chem underestimates the median FA mixing ratio most
816 significantly in smoke impacted samples, doing slightly better during low/no smoke periods in

817 the western U.S. Alternatively, GEOS-Chem does well simulating FA mixing ratios in the free
818 troposphere during all three periods, in good agreement with Chen et al.¹⁷ This is particularly
819 evident in FIREX-AQ-W free troposphere samples, which agree nearly 1:1 with the model.
820 Similarly, the model also does very well simulating median FA mixing ratios in the low/no
821 smoke southeast U.S. samples (NMB -36 %). As this profile reflects minimal smoke impact
822 during the period, it suggests that the model is accurately simulating FA from biogenic sources in
823 the southeast U.S., as reflected in recent model developments including production from
824 stabilized Criegee intermediates and acetaldehyde tautomerization as implemented by Millet et
825 al.⁷ and Chen et al.¹⁷

826
827 Although GEOS-Chem does better simulating FA during low/no smoke samples than in smoke
828 in the western U.S., the improvement is only modest with NMB decreasing by < 10 %. This may
829 in part reflect the widespread smoke impacts in the western U.S. during fire season, where a pool
830 of longer-lived oxygenated species could persist in the region.²⁴ However, it also suggests that
831 the model may be missing a FA source or secondary chemistry from biogenic precursors unique
832 to coniferous forests,¹¹ which are likely different than those most responsible for FA in the
833 southeastern U.S. For example, isoprene oxidation is thought to be one of the main contributors
834 to FA formation above deciduous forests,⁷ while in coniferous forests emissions are typically
835 dominated by monoterpenes and 2-methyl-3-buten-2-ol (MBO),⁹⁵ whose potential contribution
836 to FA formation is unclear.

837



838

839 **Figure 7.** Vertical profiles of the median formic acid mixing ratios measured during the WE-
 840 CAN field campaign for smoke impacted, low/no smoke, and free troposphere sampling periods.
 841 Pressures are binned at every 33 hPa. Black and gray lines correspond to the measurements made
 842 by I-CIMS and PTR-ToF. Red dashed lines correspond to GEOS-Chem with GFAS BB
 843 emissions (GC), orange dashed lines are GEOS-Chem with $3 \times$ GFAS BB
 844 emissions (GCx3), and the pink dotted lines are GEOS-Chem with BB emissions turned off (GC NoBB). Error bars
 845 are the 25th and 75th percentile of the I-CIMS measurement at each pressure bin.
 846

847 To explore the regional sources of FA using the two campaign datasets, Figure 8 shows how FA
 848 correlates with CO, methanol, acetone, and MVC+MACR (methyl vinyl ketone and
 849 methacrolein) in the three regions and environments shown in Figure 7. The plot of FA vs CO
 850 shows two distinct populations between the smoke and low/no smoke environments. As CO is
 851 mainly from BB in the WE-CAN and FIREX-AQ datasets, the correlation of FA with CO in
 852 smoke samples indicates FA coming from BB sources, while the spread likely represents FA
 853 enhancement relative to primary emissions. In low/no smoke samples, the FA:CO slope is
 854 steeper than in the smoke samples, suggesting a FA source that is independent of the combustion
 855 process thus pointing to photochemical origin.

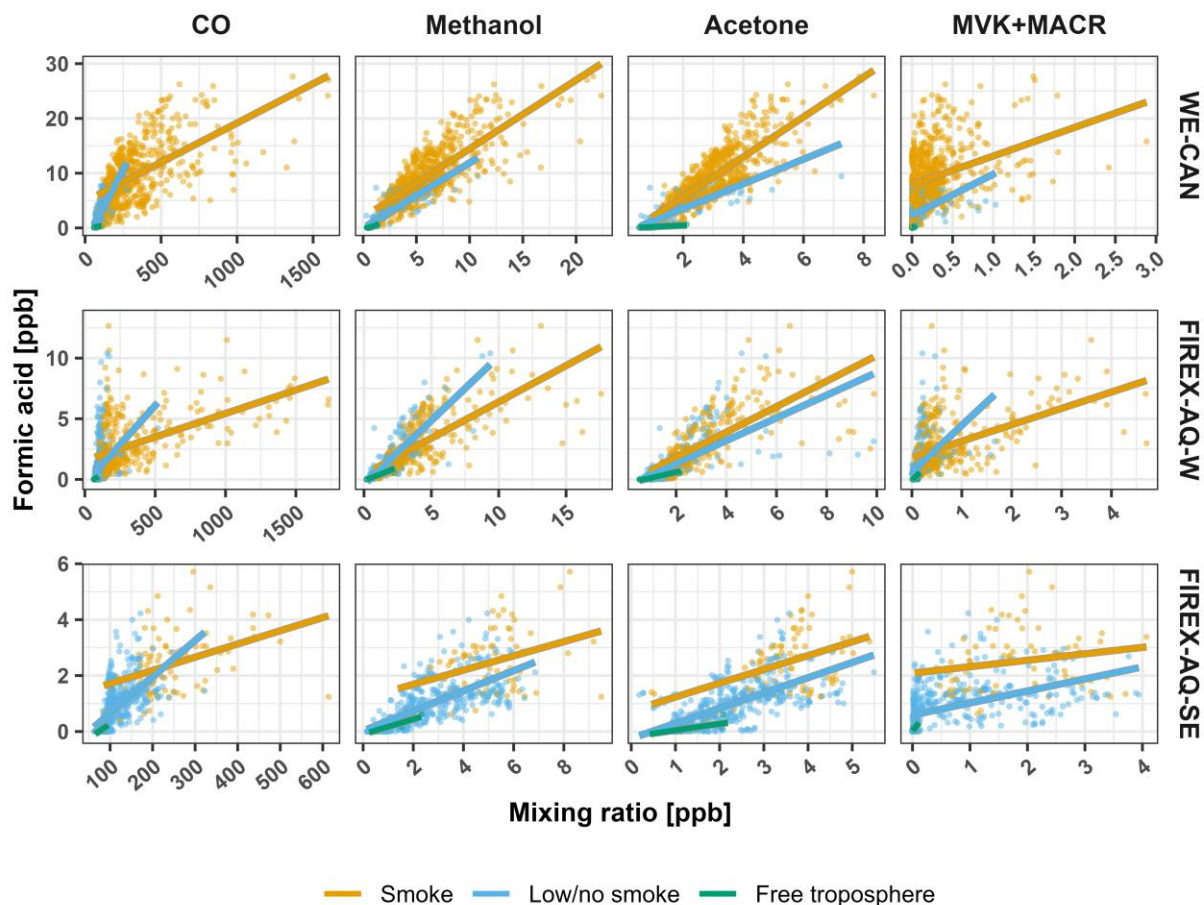
856

857 Interestingly, Figure 8 also shows that FA is well correlated with both methanol ($r^2 = 0.55\text{--}0.75$)
858 and acetone ($0.42\text{--}0.72$), with generally similar slopes in both smoke and low/no smoke samples
859 (methanol = $0.5\text{--}0.9$, acetone = $0.2\text{--}0.4$) during WE-CAN and FIREX-AQ-W periods. In
860 contrast to FA, neither methanol nor acetone measured during WE-CAN see net production in
861 the 5 smoke plumes and ~8 hours of aging discussed in Section 5 (Figure S11). This suggests
862 that their correlations in Figure 8 are not due to near-field production in BB, though
863 enhancement in much more aged plumes (> 2 days) has been observed.^{96,97} As methanol and
864 acetone are known to be major primary emissions and secondary products from biogenic
865 sources,^{12,96,98–101} we hypothesize that their strong correlation with FA during WE-CAN and
866 FIREX-AQ indicates that a portion of the observed FA may be of biogenic origin, though the
867 long atmospheric lifetimes of all three species (> 2 days) likely also play a role in why they are
868 well correlated with each other.

869

870 As isoprene is known to be the major FA precursor in deciduous forests, Figure 8 also shows FA
871 vs. MVK+MACR, an important isoprene oxidation product. During WE-CAN and FIREX-AQ,
872 FA has a weak positive correlation with MVK+MACR in most environments ($r^2 = 0.11\text{--}0.24$),
873 further indicating that some of the observed FA is indeed related to biogenic species. Some of
874 the agreement between the two is also likely due to both being primary BB emissions,¹⁸ while
875 the large spread in the correlations also points to MVK+MACR being lost as the plumes age
876 (Figure S11). Consequently, the model underestimate of FA in the western U.S. is likely due to
877 both missing secondary chemistry from BB and biogenic sources, pointing to a need for more
878 detailed studies of FA production from both BB and coniferous forest emissions.

879



880

881 **Figure 8.** Correlations of FA with CO, methanol, acetone, and MVK+MACR (methyl vinyl
 882 ketone and methacrolein) in WE-CAN and FIREX-AQ observations. Orange points represent
 883 smoke-impacted data, blue points indicate low/no smoke impact, and green points show clean
 884 free troposphere measurements (see main texts for definitions). The data have been averaged to 5
 885 minutes. Lines show the least squares regression corresponding to each set of colored points.
 886 Note that acetone is also measured with its isomer propanal.

887

888 A similar trend can be seen for acetic acid in Figure S12, where GEOS-Chem underestimates AA
 889 in both smoke-impacted and low/no smoke environments during all three sampling periods, with
 890 NMB improving by < 10 % between smoke low/no smoke conditions. Additionally, AA is better
 891 captured by the model in the clean free troposphere during WE-CAN (NMB -44 %), though the
 892 disparity is larger for both portions of FIREX-AQ (NMB -92 %). Figure S13 shows that AA is
 893 well correlated with CO across all WE-CAN and FIREX-AQ-W samples, with a slope in the
 894 range of reported ERs (WE-CAN slope = 15.8 ppb ppm_{CO}⁻¹, r² = 0.84; FIREX-AQ-W slope =
 895 11.0 ppb ppm_{CO}⁻¹, r² = 0.92). This further indicates that AA and CO in the western U.S. come

896 from the same source, likely BB. Given the lack of evidence for production of AA in the fresh
897 BB plumes sampled during WE-CAN (Section 5), near-field production is unlikely to explain the
898 low model bias, though production in plumes aged longer than those sampled during WE-CAN
899 is still possible. Additionally, the underrepresentation cannot be accounted for by BB emission
900 alone for two reasons: 1) the AA (and FA) emission ratio in the model was implemented using
901 the WE-CAN observations per Permar et al.¹⁸ and 2) the GEOS-Chem + 3 × GFAS, which
902 should account for the underestimated BB emissions per Jin et al.⁴¹ only slightly increases the
903 modeled AA. Consequently, the exact reason behind the low model bias for AA is unknown,
904 though it may be due to too large of a model sink and/or missing secondary production from long
905 lived biogenic and BB precursors.

906 **4 Conclusions**

907 Using detailed formic acid and acetic acid measurements made during the WE-CAN and FIREX-
908 AQ aircraft campaigns, we assess their emissions, chemistry, and model representation in the
909 western and southeastern U.S. FA measured by two commonly used mass spectrometers, PTR-
910 ToF and I CIMS, was found to have high measurement uncertainty during the WE-CAN
911 deployment (up to 100%) due to its humidity and temperature dependent sensitivities, inlet
912 artifacts, and instrument baseline issues. However, FA measured by two different PTR-ToF and
913 I CIMS instruments during the FIREX-AQ campaign were found to agree within their
914 measurement uncertainty. Accuracy for the FA measurement could be greatly improved by
915 reducing inlet losses via shorter sampling lines, increased flow rate, and/or reduced sampling line
916 diameter, thus reducing sample residence time in the instrument. In addition, regulating reaction
917 chamber temperatures, and performing more frequent humidity dependent calibrations and
918 instrument zeroing checks are key to improving the FA measurement quality in both instrument
919 types. Despite the high uncertainty in FA measured during WE-CAN, model underestimates of
920 FA mixing ratios were found to be much greater than the measurement uncertainty.

921
922 During WE-CAN FA ERs and EFs were found to be 9.5 ± 4.2 (1σ) ppb ppm_{CO}⁻¹ and 1.5 ± 0.60 g
923 kg⁻¹ respectively, which are 3.5 times higher than literature values. FIREX-AQ AA EFs and ERs
924 agree better with the literature, though are still often higher than the 75th percentile of literature
925 values. As FA was found to have little to no dependence on MCE or fuel type. The exact reason

926 for this discrepancy is currently unknown, though may reflect differences in emissions between
927 the larger wildfires sampled during WE-CAN and FIREX-AQ than from laboratory BB studies
928 and the smaller fires typically reported in the literature. It may also reflect some extent of early
929 plume production as the WE-CAN flights sampled 27–130 minutes downwind from the source.
930 However, extrapolating FA NEMRs measured downwind from these fires to t_0 does little to close
931 the gap between WE-CAN and literature ERs and EFs.

932
933 Analysis of 5 smoke plumes sampled in a pseudo-Lagrangian fashion finds that FA is rapidly
934 produced at $2.7 \text{ ppb ppmCO}^{-1} \text{ h}^{-1}$ during the first 8 hours of plume aging, in good agreement with
935 previous studies. However, F0AM run with explicit MCM or simplified GEOS-Chem chemistry
936 was unable to capture the observed production due to missing secondary sources. Observed FA
937 production was found to have statistically significant correlations ($p\text{-value} < 0.5$) with 94 VOCs
938 measured during WE-CAN. The oxidation of these 94 species collectively accounts for 127 ppbc
939 ppmCO^{-1} that is reacted away over the 8 hours of plume aging. This indicates that those species
940 could lose $6 \times$ more carbon than is needed to account for the observed FA production, though the
941 exact chemical pathways are often unknown.

942
943 AA ERs and EFs were found to fall within the 25th and 75th percentiles of the literature-reported
944 values, exhibiting a modest negative dependence on MCE and some fuel types. In contrast to
945 some previous studies, AA was not found to have any statistically significant production during
946 the first 8 hours of plume aging during WE-CAN, with downwind NEMRs generally in the range
947 of observed ERs. Consequently, most of the observed AA in the nearfield is likely from primary
948 emissions, though photochemical production may still be important for certain fires/fuels and in
949 more aged smoke.

950
951 GEOS-Chem simulations with updated FA and AA chemistry and emissions were performed for
952 the WE-CAN and FIREX-AQ campaigns and compared to field observations. For both
953 campaigns, FA and AA were found to be biased low in the model by $\sim 90\%$. The model does
954 slightly better simulating FA mixing ratios in no/low smoke impacted western U.S. samples, and
955 significantly better in no/low smoke periods over southeast U.S. forests. It is likely that much of
956 the low model bias for FA is due to missing secondary production from both BB and coniferous

957 forest specific biogenic sources. The factors leading the underestimate of AA are unknown, but
958 may reflect too large of a model sink and secondary production in smoke aged longer than
959 observed during WE-CAN.

960

961 **Acknowledgements:**

962 This study was supported by the U.S. National Science Foundation (AGS # 2144896, EPSCoR #
963 2242802). The 2018 WE-CAN field campaign was supported by NSF through grants AGS
964 #1650275 (U of Montana), # 1650786 (Colorado State U), # 1650288 (U of Colorado at
965 Boulder), # 1650493 (U of Wyoming), # 1652688 (U of Washington), #1748266 (U of
966 Montana), and the National Oceanic and Atmospheric Administration (Award #
967 NA17OAR4310010, Colorado State U). Dr. Dylan B. Millet acknowledges additional support
968 from NOAA (#NA22OAR4310200). This material was also based upon work supported by the
969 NCAR, which is a major facility sponsored by the NSF under Cooperative Agreement No.
970 1852977. The WE-CAN data were collected using NSF's Lower Atmosphere Observing
971 Facilities, which are managed and operated by NCAR's Earth Observing Laboratory. The
972 authors thank Dr. Delphine K. Farmer for use of the AMS measurements made during WE-CAN
973 and acknowledge high-performance computing resources and support from Cheyenne
974 (doi:10.5065/D6RX99HX) provided by the NCAR Computational and Information Systems
975 Laboratory, sponsored by the NSF, and the U of Montana's Griz Shared Computing Cluster
976 (GSCC).

977 **5 References**

- 978 1 D. J. Jacob, Chemistry of OH in remote clouds and its role in the production of formic acid and
979 peroxymonosulfate, *Journal of Geophysical Research: Atmospheres*, 1986, **91**, 9807–9826.
- 980 2 S. Metzger, N. Mihalopoulos and J. Lelieveld, Importance of mineral cations and organics in gas-aerosol
981 partitioning of reactive nitrogen compounds: case study based on MINOS results, *Atmospheric Chemistry and
982 Physics*, 2006, **6**, 2549–2567.
- 983 3 M. O. Andreae, R. W. Talbot, T. W. Andreae and R. C. Harriss, Formic and acetic acid over the central Amazon
984 region, Brazil: 1. Dry season, *Journal of Geophysical Research: Atmospheres*, 1988, **93**, 1616–1624.
- 985 4 J. N. Galloway, G. E. Likens, W. C. Keene and J. M. Miller, The composition of precipitation in remote areas of
986 the world, *Journal of Geophysical Research: Oceans*, 1982, **87**, 8771–8786.
- 987 5 W. C. Keene, J. N. Galloway and J. D. Holden Jr., Measurement of weak organic acidity in precipitation from
988 remote areas of the world, *Journal of Geophysical Research: Oceans*, 1983, **88**, 5122–5130.
- 989 6 T. Stavrakou, J.-F. Müller, J. Peeters, A. Razavi, L. Clarisse, C. Clerbaux, P.-F. Coheur, D. Hurtmans, M. De
990 Mazière, C. Vigouroux, N. M. Deutscher, D. W. T. Griffith, N. Jones and C. Paton-Walsh, Satellite evidence for
991 a large source of formic acid from boreal and tropical forests, *Nature Geoscience*, 2012, **5**, 26–30.
- 992 7 D. B. Millet, M. Baasandorj, D. K. Farmer, J. A. Thornton, K. Baumann, P. Brophy, S. Chaliyakunnel, J. A. de
993 Gouw, M. Graus, L. Hu, A. Koss, B. H. Lee, F. D. Lopez-Hilfiker, J. A. Neuman, F. Paulot, J. Peischl, I. B.

- 994 Pollack, T. B. Ryerson, C. Warneke, B. J. Williams and J. Xu, A large and ubiquitous source of atmospheric
995 formic acid, *Atmospheric Chemistry and Physics*, 2015, **15**, 6283–6304.
- 996 8 F. Paulot, D. Wunch, J. D. Crouse, G. C. Toon, D. B. Millet, P. F. DeCarlo, C. Vigouroux, N. M. Deutscher, G.
997 González Abad, J. Notholt, T. Warneke, J. W. Hannigan, C. Warneke, J. A. de Gouw, E. J. Dunlea, M. De
998 Mazière, D. W. T. Griffith, P. Bernath, J. L. Jimenez and P. O. Wennberg, Importance of secondary sources in
999 the atmospheric budgets of formic and acetic acids, *Atmospheric Chemistry and Physics*, 2011, **11**, 1989–2013.
- 1000 9 H. D. Alwe, D. B. Millet, X. Chen, J. D. Raff, Z. C. Payne and K. Fledderman, Oxidation of Volatile Organic
1001 Compounds as the Major Source of Formic Acid in a Mixed Forest Canopy, *Geophysical Research Letters*, 2019,
1002 **46**, 2940–2948.
- 1003 10 T. B. Nguyen, J. D. Crouse, A. P. Teng, J. M. S. Clair, F. Paulot, G. M. Wolfe and P. O. Wennberg, Rapid
1004 deposition of oxidized biogenic compounds to a temperate forest, *Proceedings of the National Academy of
1005 Sciences*, 2015, **112**, E392–E401.
- 1006 11 S. Schobesberger, F. D. Lopez-Hilfiker, D. Taipale, D. B. Millet, E. L. D’Ambro, P. Rantala, I. Mammarella, P.
1007 Zhou, G. M. Wolfe, B. H. Lee, M. Boy and J. A. Thornton, High upward fluxes of formic acid from a boreal
1008 forest canopy, *Geophysical Research Letters*, 2016, **43**, 9342–9351.
- 1009 12 V. Selimovic, D. Ketcherside, S. Chaliyakunnel, C. Wielgasz, W. Permar, H. Angot, D. B. Millet, A. Fried, D.
1010 Helmig and L. Hu, Atmospheric biogenic volatile organic compounds in the Alaskan Arctic tundra: constraints
1011 from measurements at Toolik Field Station, *Atmospheric Chemistry and Physics*, 2022, **22**, 14037–14058.
- 1012 13 M. Le Breton, M. R. McGillen, J. B. A. Muller, A. Bacak, D. E. Shallcross, P. Xiao, L. G. Huey, D. Tanner, H.
1013 Coe and C. J. Percival, Airborne observations of formic acid using a chemical ionization mass spectrometer,
1014 *Atmospheric Measurement Techniques*, 2012, **5**, 3029–3039.
- 1015 14 B. Yuan, P. R. Veres, C. Warneke, J. M. Roberts, J. B. Gilman, A. Koss, P. M. Edwards, M. Graus, W. C. Kuster,
1016 S.-M. Li, R. J. Wild, S. S. Brown, W. P. Dubé, B. M. Lerner, E. J. Williams, J. E. Johnson, P. K. Quinn, T. S.
1017 Bates, B. Lefer, P. L. Hayes, J. L. Jimenez, R. J. Weber, R. Zamora, B. Ervens, D. B. Millet, B. Rappenglück and
1018 J. A. de Gouw, Investigation of secondary formation of formic acid: urban environment vs. oil and gas producing
1019 region, *Atmospheric Chemistry and Physics*, 2015, **15**, 1975–1993.
- 1020 15 K. E. Cady-Pereira, S. Chaliyakunnel, M. W. Shephard, D. B. Millet, M. Luo and K. C. Wells, HCOOH
1021 measurements from space: TES retrieval algorithm and observed global distribution, *Atmospheric Measurement
1022 Techniques*, 2014, **7**, 2297–2311.
- 1023 16 S. Chaliyakunnel, D. B. Millet, K. C. Wells, K. E. Cady-Pereira and M. W. Shephard, A Large Underestimate of
1024 Formic Acid from Tropical Fires: Constraints from Space-Borne Measurements, *Environ. Sci. Technol.*, 2016,
1025 **50**, 5631–5640.
- 1026 17 X. Chen, D. B. Millet, J. A. Neuman, P. R. Veres, E. A. Ray, R. Commane, B. C. Daube, K. McKain, J. P.
1027 Schwarz, J. M. Katich, K. D. Froyd, G. P. Schill, M. J. Kim, J. D. Crouse, H. M. Allen, E. C. Apel, R. S.
1028 Hornbrook, D. R. Blake, B. A. Nault, P. Campuzano-Jost, J. L. Jimenez and J. E. Dibb, HCOOH in the Remote
1029 Atmosphere: Constraints from Atmospheric Tomography (ATom) Airborne Observations, *ACS Earth Space
1030 Chem.*, 2021, **5**, 1436–1454.
- 1031 18 W. Permar, Q. Wang, V. Selimovic, C. Wielgasz, R. J. Yokelson, R. S. Hornbrook, A. J. Hills, E. C. Apel, I.-T.
1032 Ku, Y. Zhou, B. C. Sive, A. P. Sullivan, J. L. Collett Jr, T. L. Campos, B. B. Palm, Q. Peng, J. A. Thornton, L.
1033 A. Garofalo, D. K. Farmer, S. M. Kreidenweis, E. J. T. Levin, P. J. DeMott, F. Flocke, E. V. Fischer and L. Hu,
1034 Emissions of Trace Organic Gases From Western U.S. Wildfires Based on WE-CAN Aircraft Measurements,
1035 *Journal of Geophysical Research: Atmospheres*, 2021, **126**, e2020JD033838.
- 1036 19 S. K. Akagi, J. S. Craven, J. W. Taylor, G. R. McMeeking, R. J. Yokelson, I. R. Burling, S. P. Urbanski, C. E.
1037 Wold, J. H. Seinfeld, H. Coe, M. J. Alvarado and D. R. Weise, Evolution of trace gases and particles emitted by
1038 a chaparral fire in California, *Atmos. Chem. Phys.*, 2012, **12**, 1397–1421.
- 1039 20 J. G. Goode, R. J. Yokelson, D. E. Ward, R. A. Susott, R. E. Babbitt, M. A. Davies and W. M. Hao, Measurements
1040 of excess O₃, CO₂, CO, CH₄, C₂H₄, C₂H₂, HCN, NO, NH₃, HCOOH, CH₃COOH, HCHO, and CH₃OH in
1041 1997 Alaskan biomass burning plumes by airborne Fourier transform infrared spectroscopy (AFTIR), *Journal of
1042 Geophysical Research: Atmospheres*, 2000, **105**, 22147–22166.
- 1043 21 M. Grutter, N. Glatthor, G. P. Stiller, H. Fischer, U. Grabowski, M. Höpfner, S. Kellmann, A. Linden and T. von
1044 Clarmann, Global distribution and variability of formic acid as observed by MIPAS-ENVISAT, *Journal of
1045 Geophysical Research: Atmospheres*, , DOI:https://doi.org/10.1029/2009JD012980.
- 1046 22 R. J. Yokelson, J. D. Crouse, P. F. DeCarlo, T. Karl, S. Urbanski, E. Atlas, T. Campos, Y. Shinozuka, V.
1047 Kapustin, A. D. Clarke, A. Weinheimer, D. J. Knapp, D. D. Montzka, J. Holloway, P. Weibring, F. Flocke, W.
1048 Zheng, D. Toohey, P. O. Wennberg, C. Wiedinmyer, L. Mauldin, A. Fried, D. Richter, J. Walega, J. L. Jimenez,

- 1049 K. Adachi, P. R. Buseck, S. R. Hall and R. Shetter, Emissions from biomass burning in the Yucatan, *Atmospheric*
1050 *Chemistry and Physics*, 2009, **9**, 5785–5812.
- 1051 23 R. J. Yokelson, J. G. Goode, D. E. Ward, R. A. Susott, R. E. Babbitt, D. D. Wade, I. Bertschi, D. W. T. Griffith
1052 and W. M. Hao, Emissions of formaldehyde, acetic acid, methanol, and other trace gases from biomass fires in
1053 North Carolina measured by airborne Fourier transform infrared spectroscopy, *Journal of Geophysical Research:*
1054 *Atmospheres*, 1999, **104**, 30109–30125.
- 1055 24 W. Permar, L. Jin, Q. Peng, K. O'Dell, E. Lill, V. Selimovic, R. J. Yokelson, R. S. Hornbrook, A. J. Hills, E. C.
1056 Apel, I.-T. Ku, Y. Zhou, B. C. Sive, A. P. Sullivan, J. L. Collett, B. B. Palm, J. A. Thornton, F. Flocke, E. V.
1057 Fischer and L. Hu, Atmospheric OH reactivity in the western United States determined from comprehensive gas-
1058 phase measurements during WE-CAN, *Environ. Sci.: Atmos.*, 2023, **3**, 97–114.
- 1059 25 A. R. Koss, K. Sekimoto, J. B. Gilman, V. Selimovic, M. M. Coggon, K. J. Zarzana, B. Yuan, B. M. Lerner, S.
1060 S. Brown, J. L. Jimenez, J. Krechmer, J. M. Roberts, C. Warneke, R. J. Yokelson and J. de Gouw, Non-methane
1061 organic gas emissions from biomass burning: identification, quantification, and emission factors from PTR-ToF
1062 during the FIREX 2016 laboratory experiment, *Atmos. Chem. Phys.*, 2018, **18**, 3299–3319.
- 1063 26 R. J. Yokelson, I. T. Bertschi, T. J. Christian, P. V. Hobbs, D. E. Ward and W. M. Hao, Trace gas measurements
1064 in nascent, aged, and cloud-processed smoke from African savanna fires by airborne Fourier transform infrared
1065 spectroscopy (AFTIR), *Journal of Geophysical Research: Atmospheres*, ,
1066 DOI:<https://doi.org/10.1029/2002JD002322>.
- 1067 27 A. Chebbi and P. Carlier, Carboxylic acids in the troposphere, occurrence, sources, and sinks: A review,
1068 *Atmospheric Environment*, 1996, **30**, 4233–4249.
- 1069 28 J.-F. Müller, T. Stavroukou and J. Peeters, Chemistry and deposition in the Model of Atmospheric composition at
1070 Global and Regional scales using Inversion Techniques for Trace gas Emissions (MAGRITTE v1.1) – Part 1:
1071 Chemical mechanism, *Geoscientific Model Development*, 2019, **12**, 2307–2356.
- 1072 29 U. Baltensperger, M. Kalberer, J. Dommen, D. Paulsen, M. R. Alfarra, H. Coe, R. Fisseha, A. Gascho, M. Gysel,
1073 S. Nyeki, M. Sax, M. Steinbacher, A. S. H. Prevot, S. Sjögren, E. Weingartner and R. Zenobi, Secondary organic
1074 aerosols from anthropogenic and biogenic precursors, *Faraday Discuss.*, 2005, **130**, 265–278.
- 1075 30 K. P. Wyche, P. S. Monks, A. M. Ellis, R. L. Cordell, A. E. Parker, C. Whyte, A. Metzger, J. Dommen, J.
1076 Duplissy, A. S. H. Prevot, U. Baltensperger, A. R. Rickard and F. Wulfert, Gas phase precursors to anthropogenic
1077 secondary organic aerosol: detailed observations of 1,3,5-trimethylbenzene photooxidation, *Atmospheric*
1078 *Chemistry and Physics*, 2009, **9**, 635–665.
- 1079 31 A. Bossolasco, E. P. Faragó, C. Schoemaeker and C. Fittschen, Rate constant of the reaction between CH₃O₂
1080 and OH radicals, *Chemical Physics Letters*, 2014, **593**, 7–13.
- 1081 32 B. Franco, T. Blumenstock, C. Cho, L. Clarisse, C. Clerbaux, P.-F. Coheur, M. De Mazière, I. De Smedt, H.-P.
1082 Dorn, T. Emmerichs, H. Fuchs, G. Gkatzelis, D. W. T. Griffith, S. Gromov, J. W. Hannigan, F. Hase, T. Hohaus,
1083 N. Jones, A. Kerkweg, A. Kiendler-Scharr, E. Lutsch, E. Mahieu, A. Novelli, I. Ortega, C. Paton-Walsh, M.
1084 Pommier, A. Pozzer, D. Reimer, S. Rosanka, R. Sander, M. Schneider, K. Strong, R. Tillmann, M. Van
1085 Roozendaal, L. Vereecken, C. Vigouroux, A. Wahner and D. Taraborrelli, Ubiquitous atmospheric production of
1086 organic acids mediated by cloud droplets, *Nature*, 2021, **593**, 233–237.
- 1087 33 J. D. Cope, K. A. Abellar, K. H. Bates, X. Fu and T. B. Nguyen, Aqueous Photochemistry of 2-Methyltetrol and
1088 Erythritol as Sources of Formic Acid and Acetic Acid in the Atmosphere, *ACS Earth Space Chem.*, 2021, **5**,
1089 1265–1277.
- 1090 34 M. Müller, B. E. Anderson, A. J. Beyersdorf, J. H. Crawford, G. S. Diskin, P. Eichler, A. Fried, F. N. Keutsch,
1091 T. Mikoviny, K. L. Thornhill, J. G. Walega, A. J. Weinheimer, M. Yang, R. J. Yokelson and A. Wisthaler, In situ
1092 measurements and modeling of reactive trace gases in a small biomass burning plume, *Atmos. Chem. Phys.*, 2016,
1093 **16**, 3813–3824.
- 1094 35 S. K. Akagi, R. J. Yokelson, I. R. Burling, S. Meinardi, I. Simpson, D. R. Blake, G. R. McMeeking, A. Sullivan,
1095 T. Lee, S. Kreidenweis, S. Urbanski, J. Reardon, D. W. T. Griffith, T. J. Johnson and D. R. Weise, Measurements
1096 of reactive trace gases and variable O₃ formation rates in some South Carolina biomass burning plumes,
1097 *Atmospheric Chemistry and Physics*, 2013, **13**, 1141–1165.
- 1098 36 J. Trentmann, R. J. Yokelson, P. V. Hobbs, T. Winterrath, T. J. Christian, M. O. Andreae and S. A. Mason, An
1099 analysis of the chemical processes in the smoke plume from a savanna fire, *Journal of Geophysical Research:*
1100 *Atmospheres*, , DOI:<https://doi.org/10.1029/2004JD005628>.
- 1101 37 S. R. Fulgham, P. Brophy, M. Link, J. Ortega, I. Pollack and D. K. Farmer, Seasonal Flux Measurements over a
1102 Colorado Pine Forest Demonstrate a Persistent Source of Organic Acids, *ACS Earth Space Chem.*, 2019, **3**, 2017–
1103 2032.

- 1104 38 X. Lee, D. Huang, Q. Liu, X. Liu, H. Zhou, Q. Wang and Y. Ma, Underrated primary biogenic origin and lifetime
1105 of atmospheric formic and acetic acid, *Scientific Reports*, 2021, **11**, 7176.
- 1106 39 M. F. Shaw, B. Sztáray, L. K. Whalley, D. E. Heard, D. B. Millet, M. J. T. Jordan, D. L. Osborn and S. H. Kable,
1107 Photo-tautomerization of acetaldehyde as a photochemical source of formic acid in the troposphere, *Nature*
1108 *Communications*, 2018, **9**, 2584.
- 1109 40 C. Warneke, J. P. Schwarz, J. Dibb, O. Kalashnikova, G. Frost, J. Al-Saad, S. S. Brown, Wm. A. Brewer, A.
1110 Soja, F. C. Seidel, R. A. Washenfelder, E. B. Wiggins, R. H. Moore, B. E. Anderson, C. Jordan, T. I. Yacovitch,
1111 S. C. Herndon, S. Liu, T. Kuwayama, D. Jaffe, N. Johnston, V. Selimovic, R. Yokelson, D. M. Giles, B. N.
1112 Holben, P. Goloub, I. Popovici, M. Trainer, A. Kumar, R. B. Pierce, D. Fahey, J. Roberts, E. M. Gargulinski, D.
1113 A. Peterson, X. Ye, L. H. Thapa, P. E. Saide, C. H. Fite, C. D. Holmes, S. Wang, M. M. Coggon, Z. C. J. Decker,
1114 C. E. Stockwell, L. Xu, G. Gkatzelis, K. Aikin, B. Lefer, J. Kaspari, D. Griffin, L. Zeng, R. Weber, M. Hastings,
1115 J. Chai, G. M. Wolfe, T. F. Hanisco, J. Liao, P. Campuzano Jost, H. Guo, J. L. Jimenez, J. Crawford and T. F.-
1116 A. S. Team, Fire Influence on Regional to Global Environments and Air Quality (FIREX-AQ), *Journal of*
1117 *Geophysical Research: Atmospheres*, 2023, **128**, e2022JD037758.
- 1118 41 L. Jin, W. Permar, V. Selimovic, D. Ketcherside, R. J. Yokelson, R. S. Hornbrook, E. C. Apel, I.-T. Ku, J. L.
1119 Collett Jr., A. P. Sullivan, D. A. Jaffe, J. R. Pierce, A. Fried, M. M. Coggon, G. I. Gkatzelis, C. Warneke, E. V.
1120 Fischer and L. Hu, Constraining emissions of volatile organic compounds from western US wildfires with WE-
1121 CAN and FIREX-AQ airborne observations, *Atmospheric Chemistry and Physics*, 2023, **23**, 5969–5991.
- 1122 42 NIFC, <https://www.nifc.gov/fire-information/statistics/wildfires>, (accessed 7 February 2023).
- 1123 43 B. H. Lee, F. D. Lopez-Hilfiker, C. Mohr, T. Kurtén, D. R. Worsnop and J. A. Thornton, An Iodide-Adduct High-
1124 Resolution Time-of-Flight Chemical-Ionization Mass Spectrometer: Application to Atmospheric Inorganic and
1125 Organic Compounds, *Environ. Sci. Technol.*, 2014, **48**, 6309–6317.
- 1126 44 B. H. Lee, F. D. Lopez-Hilfiker, P. R. Veres, E. E. McDuffie, D. L. Fibiger, T. L. Sparks, C. J. Ebben, J. R.
1127 Green, J. C. Schroder, P. Campuzano-Jost, S. Iyer, E. L. D’Ambro, S. Schobesberger, S. S. Brown, P. J.
1128 Wooldridge, R. C. Cohen, M. N. Fiddler, S. Bililign, J. L. Jimenez, T. Kurtén, A. J. Weinheimer, L. Jaegle and
1129 J. A. Thornton, Flight Deployment of a High-Resolution Time-of-Flight Chemical Ionization Mass Spectrometer:
1130 Observations of Reactive Halogen and Nitrogen Oxide Species, *Journal of Geophysical Research: Atmospheres*,
1131 2018, **123**, 7670–7686.
- 1132 45 B. B. Palm, X. Liu, J. L. Jimenez and J. A. Thornton, Performance of a new coaxial ion–molecule reaction region
1133 for low-pressure chemical ionization mass spectrometry with reduced instrument wall interactions, *Atmos. Meas.*
1134 *Tech.*, 2019, **12**, 5829–5844.
- 1135 46 Q. Peng, B. B. Palm, K. E. Melander, B. H. Lee, S. R. Hall, K. Ullmann, T. Campos, A. J. Weinheimer, E. C.
1136 Apel, R. S. Hornbrook, A. J. Hills, D. D. Montzka, F. Flocke, L. Hu, W. Permar, C. Wielgasz, J. Lindaas, I. B.
1137 Pollack, E. V. Fischer, T. H. Bertram and J. A. Thornton, HONO Emissions from Western U.S. Wildfires Provide
1138 Dominant Radical Source in Fresh Wildfire Smoke, *Environ. Sci. Technol.*, 2020, **54**, 5954–5963.
- 1139 47 I. Bourgeois, J. Peischl, J. A. Neuman, S. S. Brown, H. M. Allen, P. Campuzano-Jost, M. M. Coggon, J. P.
1140 DiGangi, G. S. Diskin, J. B. Gilman, G. I. Gkatzelis, H. Guo, H. A. Halliday, T. F. Hanisco, C. D. Holmes, L. G.
1141 Huey, J. L. Jimenez, A. D. Lamplugh, Y. R. Lee, J. Lindaas, R. H. Moore, B. A. Nault, J. B. Nowak, D. Pagonis,
1142 P. S. Rickly, M. A. Robinson, A. W. Rollins, V. Selimovic, J. M. St. Clair, D. Tanner, K. T. Vasquez, P. R. Veres,
1143 C. Warneke, P. O. Wennberg, R. A. Washenfelder, E. B. Wiggins, C. C. Womack, L. Xu, K. J. Zarzana and T.
1144 B. Ryerson, Comparison of airborne measurements of NO, NO₂, HONO, NO_y, and CO during FIREX-AQ,
1145 *Atmospheric Measurement Techniques*, 2022, **15**, 4901–4930.
- 1146 48 M. A. Robinson, J. A. Neuman, L. G. Huey, J. M. Roberts, S. S. Brown and P. R. Veres, Temperature-dependent
1147 sensitivity of iodide chemical ionization mass spectrometers, *Atmospheric Measurement Techniques*, 2022, **15**,
1148 4295–4305.
- 1149 49 L. A. Garofalo, M. A. Pothier, E. J. T. Levin, T. Campos, S. M. Kreidenweis and D. K. Farmer, Emission and
1150 Evolution of Submicron Organic Aerosol in Smoke from Wildfires in the Western United States, *ACS Earth*
1151 *Space Chem.*, 2019, **3**, 1237–1247.
- 1152 50 M. J. Cubison, A. M. Ortega, P. L. Hayes, D. K. Farmer, D. Day, M. J. Lechner, W. H. Brune, E. Apel, G. S.
1153 Diskin, J. A. Fisher, H. E. Fuelberg, A. Hecobian, D. J. Knapp, T. Mikoviny, D. Riemer, G. W. Sachse, W.
1154 Sessions, R. J. Weber, A. J. Weinheimer, A. Wisthaler and J. L. Jimenez, Effects of aging on organic aerosol
1155 from open biomass burning smoke in aircraft and laboratory studies, *Atmospheric Chemistry and Physics*, 2011,
1156 **11**, 12049–12064.
- 1157 51 J. L. Jimenez, M. R. Canagaratna, N. M. Donahue, A. S. H. Prevot, Q. Zhang, J. H. Kroll, P. F. DeCarlo, J. D.
1158 Allan, H. Coe, N. L. Ng, A. C. Aiken, K. S. Docherty, I. M. Ulbrich, A. P. Grieshop, A. L. Robinson, J. Duplissy,
1159 J. D. Smith, K. R. Wilson, V. A. Lanz, C. Hueglin, Y. L. Sun, J. Tian, A. Laaksonen, T. Raatikainen, J. Rautiainen,

1160 P. Vaattovaara, M. Ehn, M. Kulmala, J. M. Tomlinson, D. R. Collins, M. J. Cubison, E., J. Dunlea, J. A. Huffman,
1161 T. B. Onasch, M. R. Alfarra, P. I. Williams, K. Bower, Y. Kondo, J. Schneider, F. Drewnick, S. Borrmann, S.
1162 Weimer, K. Demerjian, D. Salcedo, L. Cottrell, R. Griffin, A. Takami, T. Miyoshi, S. Hatakeyama, A. Shimono,
1163 J. Y. Sun, Y. M. Zhang, K. Dzepina, J. R. Kimmel, D. Sueper, J. T. Jayne, S. C. Herndon, A. M. Trimborn, L. R.
1164 Williams, E. C. Wood, A. M. Middlebrook, C. E. Kolb, U. Baltensperger and D. R. Worsnop, Evolution of
1165 Organic Aerosols in the Atmosphere, *Science*, 2009, **326**, 1525–1529.

1166 52 J. L. Jimenez, P. Campuzano-Jost, D. A. Day, B. A. Nault, H. Guo, J. C. Schroder and M. J. Cubison, Frequently
1167 Asked AMS Questions for AMS Data Users, [http://cires1.colorado.edu/jimenez-](http://cires1.colorado.edu/jimenez-group/wiki/index.php/FAQ_for_AMS_Data_Users)
1168 [group/wiki/index.php/FAQ_for_AMS_Data_Users](http://cires1.colorado.edu/jimenez-group/wiki/index.php/FAQ_for_AMS_Data_Users), (accessed 10 June 2023).

1169 53 M. Baasandorj, D. B. Millet, L. Hu, D. Mitroo and B. J. Williams, Measuring acetic and formic acid by proton-
1170 transfer-reaction mass spectrometry: sensitivity, humidity dependence, and quantifying interferences, *Atmos.*
1171 *Meas. Tech.*, 2015, **8**, 1303–1321.

1172 54 J. A. de Gouw and C. Warneke, Measurements of volatile organic compounds in the earth’s atmosphere using
1173 proton-transfer-reaction mass spectrometry, *Mass Spectrom. Rev.*, 2007, **26**, 223–257.

1174 55 B. Yuan, A. R. Koss, C. Warneke, M. Coggon, K. Sekimoto and J. A. de Gouw, Proton-Transfer-Reaction Mass
1175 Spectrometry: Applications in Atmospheric Sciences, *Chem. Rev.*, 2017, **117**, 13187–13229.

1176 56 E. C. Fortner, J. Zheng, R. Zhang, W. Berk Knighton, R. M. Volkamer, P. Sheehy, L. Molina and M. André,
1177 Measurements of Volatile Organic Compounds Using Proton Transfer Reaction – Mass Spectrometry during the
1178 MILAGRO 2006 Campaign, *Atmospheric Chemistry and Physics*, 2009, **9**, 467–481.

1179 57 J. B. Gilman, B. M. Lerner, W. C. Kuster, P. D. Goldan, C. Warneke, P. R. Veres, J. M. Roberts, J. A. de Gouw,
1180 I. R. Burling and R. J. Yokelson, Biomass burning emissions and potential air quality impacts of volatile organic
1181 compounds and other trace gases from fuels common in the US, *Atmos. Chem. Phys.*, 2015, **15**, 13915–13938.

1182 58 P. Španěl, A. M. Diskin, T. Wang and D. Smith, A SIFT study of the reactions of H₃O⁺, NO⁺ and O₂⁺ with
1183 hydrogen peroxide and peroxyacetic acid, *International Journal of Mass Spectrometry*, 2003, **228**, 269–283.

1184 59 R. J. Yokelson, R. Susott, D. E. Ward, J. Reardon and D. W. T. Griffith, Emissions from smoldering combustion
1185 of biomass measured by open-path Fourier transform infrared spectroscopy, *Journal of Geophysical Research:*
1186 *Atmospheres*, 1997, **102**, 18865–18877.

1187 60 D. J. Marino, in *Encyclopedia of Toxicology (Second Edition)*, ed. P. Wexler, Elsevier, New York, Second
1188 Edition., 2005, pp. 277–279.

1189 61 L. E. Hatch, W. Luo, J. F. Pankow, R. J. Yokelson, C. E. Stockwell and K. C. Barsanti, Identification and
1190 quantification of gaseous organic compounds emitted from biomass burning using two-dimensional gas
1191 chromatography–time-of-flight mass spectrometry, *Atmospheric Chemistry and Physics*, 2015, **15**, 1865–1899.

1192 62 T. J. Christian, B. Kleiss, R. J. Yokelson, R. Holzinger, P. J. Crutzen, W. M. Hao, T. Shirai and D. R. Blake,
1193 Comprehensive laboratory measurements of biomass-burning emissions: 2. First intercomparison of open-path
1194 FTIR, PTR-MS, and GC-MS/FID/ECD, *Journal of Geophysical Research: Atmospheres*, ,
1195 DOI:<https://doi.org/10.1029/2003JD003874>.

1196 63 V. Selimovic, R. J. Yokelson, C. Warneke, J. M. Roberts, J. de Gouw, J. Reardon and D. W. T. Griffith, Aerosol
1197 optical properties and trace gas emissions by PAX and OP-FTIR for laboratory-simulated western US wildfires
1198 during FIREX, *Atmos. Chem. Phys.*, 2018, **18**, 2929–2948.

1199 64 C. Bacher, G. S. Tyndall and J. J. Orlando, The Atmospheric Chemistry of Glycolaldehyde, *Journal of*
1200 *Atmospheric Chemistry*, 2001, **39**, 171–189.

1201 65 P. Veres, J. B. Gilman, J. M. Roberts, W. C. Kuster, C. Warneke, I. R. Burling and J. de Gouw, Development
1202 and validation of a portable gas phase standard generation and calibration system for volatile organic compounds,
1203 *Atmos. Meas. Tech.*, 2010, **3**, 683–691.

1204 66 I. Bey, D. J. Jacob, R. M. Yantosca, J. A. Logan, B. D. Field, A. M. Fiore, Q. Li, H. Y. Liu, L. J. Mickley and M.
1205 G. Schultz, Global modeling of tropospheric chemistry with assimilated meteorology: Model description and
1206 evaluation, *Journal of Geophysical Research: Atmospheres*, 2001, **106**, 23073–23095.

1207 67 The International GEOS-Chem User Community, 2018.

1208 68 P. V. Hobbs, P. Sinha, R. J. Yokelson, T. J. Christian, D. R. Blake, S. Gao, T. W. Kirchstetter, T. Novakov and
1209 P. Pilewskie, Evolution of gases and particles from a savanna fire in South Africa, *Journal of Geophysical*
1210 *Research: Atmospheres*, 2003, **108**, 8485.

1211 69 J. Lindaas, I. B. Pollack, L. A. Garofalo, M. A. Pothier, D. K. Farmer, S. M. Kreidenweis, T. L. Campos, F.
1212 Flocke, A. J. Weinheimer, D. D. Montzka, G. S. Tyndall, B. B. Palm, Q. Peng, J. A. Thornton, W. Permar, C.
1213 Wielgasz, L. Hu, R. D. Ottmar, J. C. Restaino, A. T. Hudak, I.-T. Ku, Y. Zhou, B. C. Sive, A. Sullivan, J. L.
1214 Collett Jr and E. V. Fischer, Emissions of Reactive Nitrogen From Western U.S. Wildfires During Summer 2018,
1215 *Journal of Geophysical Research: Atmospheres*, 2021, **126**, e2020JD032657.

1216 70 C. R. Lonsdale, M. J. Alvarado, A. L. Hodshire, E. Ramnarine and J. R. Pierce, Simulating the forest fire plume
1217 dispersion, chemistry, and aerosol formation using SAM-ASP version 1.0, *Geoscientific Model Development*,
1218 2020, **13**, 4579–4593.

1219 71 R. J. Yokelson, D. W. T. Griffith and D. E. Ward, Open-path Fourier transform infrared studies of large-scale
1220 laboratory biomass fires, *Journal of Geophysical Research: Atmospheres*, 1996, **101**, 21067–21080.

1221 72 C. Wielgasz, Investigation of emissions and chemistry of formic acid and acetic acid in wildfire smoke., *Graduate*
1222 *Student Theses, Dissertations, & Professional Papers*.

1223 73 S. J. Prichard, S. M. O’Neill, P. Eagle, A. G. Andreu, B. Drye, J. Dubowy, S. Urbanski and T. M. Strand, Wildland
1224 fire emission factors in North America: synthesis of existing data, measurement needs and management
1225 applications, *Int. J. Wildland Fire*, 2020, **29**, 132.

1226 74 R. J. Yokelson, S. K. Akagi, D. W. T. Griffith and T. J. Johnson, Interactive comment on “Exceptional emissions
1227 of NH₃ and HCOOH in the 2010 Russian wildfires” by Y. R’Honiet al., *Atmos. Chem. Phys. Discuss.*, 2013, **12**,
1228 C11864–C11868.

1229 75 C. E. Stockwell, P. R. Veres, J. Williams and R. J. Yokelson, Characterization of biomass burning emissions
1230 from cooking fires, peat, crop residue, and other fuels with high-resolution proton-transfer-reaction time-of-flight
1231 mass spectrometry, *Atmos. Chem. Phys.*, 2015, **15**, 845–865.

1232 76 I. Bertschi, R. J. Yokelson, D. E. Ward, R. E. Babbitt, R. A. Susott, J. G. Goode and W. M. Hao, Trace gas and
1233 particle emissions from fires in large diameter and belowground biomass fuels, *Journal of Geophysical Research:*
1234 *Atmospheres*, , DOI:10.1029/2002JD002100.

1235 77 T. J. Christian, B. Kleiss, R. J. Yokelson, R. Holzinger, P. J. Crutzen, W. M. Hao, B. H. Saharjo and D. E. Ward,
1236 Comprehensive laboratory measurements of biomass-burning emissions: 1. Emissions from Indonesian, African,
1237 and other fuels, *Journal of Geophysical Research: Atmospheres*, , DOI:10.1029/2003JD003704.

1238 78 L. M. McKenzie, W. Min. Hao, G. N. Richards and D. E. Ward, Measurement and Modeling of Air Toxins from
1239 Smoldering Combustion of Biomass, *Environmental Science & Technology*, 1995, **29**, 2047–2054.

1240 79 S. K. Akagi, R. J. Yokelson, C. Wiedinmyer, M. J. Alvarado, J. S. Reid, T. Karl, J. D. Crouse and P. O.
1241 Wennberg, Emission factors for open and domestic biomass burning for use in atmospheric models, *Atmos. Chem.*
1242 *Phys.*, 2011, **11**, 4039–4072.

1243 80 J. A. de Gouw, C. Warneke, A. Stohl, A. G. Wollny, C. A. Brock, O. R. Cooper, J. S. Holloway, M. Trainer, F.
1244 C. Fehsenfeld, E. L. Atlas, S. G. Donnelly, V. Stroud and A. Lueb, Volatile organic compounds composition of
1245 merged and aged forest fire plumes from Alaska and western Canada, *Journal of Geophysical Research:*
1246 *Atmospheres*, , DOI:https://doi.org/10.1029/2005JD006175.

1247 81 G. M. Wolfe, M. R. Marvin, S. J. Roberts, K. R. Travis and J. Liao, The Framework for 0-D Atmospheric
1248 Modeling (F0AM) v3.1, *Geoscientific Model Development*, 2016, **9**, 3309–3319.

1249 82 J. Lindaas, I. B. Pollack, J. J. Calahorrano, K. O’Dell, L. A. Garofalo, M. A. Pothier, D. K. Farmer, S. M.
1250 Kreidenweis, T. Campos, F. Flocke, A. J. Weinheimer, D. D. Montzka, G. S. Tyndall, E. C. Apel, A. J. Hills, R.
1251 S. Hornbrook, B. B. Palm, Q. Peng, J. A. Thornton, W. Permar, C. Wielgasz, L. Hu, J. R. Pierce, J. L. Collett Jr.,
1252 A. P. Sullivan and E. V. Fischer, Empirical Insights Into the Fate of Ammonia in Western U.S. Wildfire Smoke
1253 Plumes, *Journal of Geophysical Research: Atmospheres*, 2021, **126**, e2020JD033730.

1254 83 B. B. Palm, Q. Peng, S. R. Hall, K. Ullmann, T. L. Campos, A. Weinheimer, D. Montzka, G. Tyndall, W. Permar,
1255 L. Hu, F. Flocke, E. V. Fischer and J. A. Thornton, Spatially Resolved Photochemistry Impacts Emissions
1256 Estimates in Fresh Wildfire Plumes, *Geophysical Research Letters*, 2021, **48**, e2021GL095443.

1257 84 B. B. Palm, Q. Peng, C. D. Fredrickson, B. H. Lee, L. A. Garofalo, M. A. Pothier, S. M. Kreidenweis, D. K.
1258 Farmer, R. P. Pokhrel, Y. Shen, S. M. Murphy, W. Permar, L. Hu, T. L. Campos, S. R. Hall, K. Ullmann, X.
1259 Zhang, F. Flocke, E. V. Fischer and J. A. Thornton, Quantification of organic aerosol and brown carbon evolution
1260 in fresh wildfire plumes, *Proceedings of the National Academy of Sciences*, 2020, **117**, 29469–29477.

1261 85 Q. Peng, B. B. Palm, C. D. Fredrickson, B. H. Lee, S. R. Hall, K. Ullmann, T. Campos, A. J. Weinheimer, E. C.
1262 Apel, F. Flocke, W. Permar, L. Hu, L. A. Garofalo, M. A. Pothier, D. K. Farmer, I.-T. Ku, A. P. Sullivan, J. L.
1263 Collett, E. Fischer and J. A. Thornton, Observations and Modeling of NO_x Photochemistry and Fate in Fresh
1264 Wildfire Plumes, *ACS Earth Space Chem.*, 2021, **5**, 2652–2667.

1265 86 M. M. Coggon, C. Y. Lim, A. R. Koss, K. Sekimoto, B. Yuan, J. B. Gilman, D. H. Hagan, V. Selimovic, K. J.
1266 Zarzana, S. S. Brown, J. M. Roberts, M. Müller, R. Yokelson, A. Wisthaler, J. E. Krechmer, J. L. Jimenez, C.
1267 Cappa, J. H. Kroll, J. de Gouw and C. Warneke, OH chemistry of non-methane organic gases (NMOGs) emitted
1268 from laboratory and ambient biomass burning smoke: evaluating the influence of furans and oxygenated
1269 aromatics on ozone and secondary NMOG formation, *Atmospheric Chemistry and Physics*, 2019, **19**, 14875–
1270 14899.

1271 87 Z. C. J. Decker, K. J. Zarzana, M. Coggon, K.-E. Min, I. Pollack, T. B. Ryerson, J. Peischl, P. Edwards, W. P.
1272 Dubé, M. Z. Markovic, J. M. Roberts, P. R. Veres, M. Graus, C. Warneke, J. de Gouw, L. E. Hatch, K. C. Barsanti
1273 and S. S. Brown, Nighttime Chemical Transformation in Biomass Burning Plumes: A Box Model Analysis
1274 Initialized with Aircraft Observations, *Environ. Sci. Technol.*, 2019, **53**, 2529–2538.
1275 88 Leeds MCM, <http://mcm.leeds.ac.uk/MCM>, (accessed 5 May 2023).
1276 89 J. Jiang, W. P. L. Carter, D. R. Cocker and K. C. Barsanti, Development and Evaluation of a Detailed Mechanism
1277 for Gas-Phase Atmospheric Reactions of Furans, *ACS Earth Space Chem.*, 2020, **4**, 1254–1268.
1278 90 M. R. Canagaratna, J. L. Jimenez, J. H. Kroll, Q. Chen, S. H. Kessler, P. Massoli, L. Hildebrandt Ruiz, E. Fortner,
1279 L. R. Williams, K. R. Wilson, J. D. Surratt, N. M. Donahue, J. T. Jayne and D. R. Worsnop, Elemental ratio
1280 measurements of organic compounds using aerosol mass spectrometry: characterization, improved calibration,
1281 and implications, *Atmospheric Chemistry and Physics*, 2015, **15**, 253–272.
1282 91 A. C. Aiken, P. F. DeCarlo, J. H. Kroll, D. R. Worsnop, J. A. Huffman, K. S. Docherty, I. M. Ulbrich, C. Mohr,
1283 J. R. Kimmel, D. Sueper, Y. Sun, Q. Zhang, A. Trimborn, M. Northway, P. J. Ziemann, M. R. Canagaratna, T.
1284 B. Onasch, M. R. Alfarra, A. S. H. Prevot, J. Dommen, J. Duplissy, A. Metzger, U. Baltensperger and J. L.
1285 Jimenez, O/C and OM/OC Ratios of Primary, Secondary, and Ambient Organic Aerosols with High-Resolution
1286 Time-of-Flight Aerosol Mass Spectrometry, *Environ. Sci. Technol.*, 2008, **42**, 4478–4485.
1287 92 C. E. Stockwell, M. M. Bela, M. M. Coggon, G. I. Gkatzelis, E. Wiggins, E. M. Gargulinski, T. Shingler, M.
1288 Fenn, D. Griffin, C. D. Holmes, X. Ye, P. E. Saide, I. Bourgeois, J. Peischl, C. C. Womack, R. A. Washenfelder,
1289 P. R. Veres, J. A. Neuman, J. B. Gilman, A. Lamplugh, R. H. Schwantes, S. A. McKeen, A. Wisthaler, F. Piel,
1290 H. Guo, P. Campuzano-Jost, J. L. Jimenez, A. Fried, T. F. Hanisco, L. G. Huey, A. Perring, J. M. Katich, G. S.
1291 Diskin, J. B. Nowak, T. P. Bui, H. S. Halliday, J. P. DiGangi, G. Pereira, E. P. James, R. Ahmadov, C. A.
1292 McLinden, A. J. Soja, R. H. Moore, J. W. Hair and C. Warneke, Airborne Emission Rate Measurements Validate
1293 Remote Sensing Observations and Emission Inventories of Western U.S. Wildfires, *Environ. Sci. Technol.*, 2022,
1294 **56**, 7564–7577.
1295 93 Y. Chen, Q. Li, J. T. Randerson, E. A. Lyons, R. A. Kahn, D. L. Nelson and D. J. Diner, The sensitivity of CO
1296 and aerosol transport to the temporal and vertical distribution of North American boreal fire emissions,
1297 *Atmospheric Chemistry and Physics*, 2009, 6559–6580.
1298 94 Y. Jian and T.-M. Fu, Injection heights of springtime biomass-burning plumes over peninsular Southeast Asia
1299 and their impacts on long-range pollutant transport, *Atmospheric Chemistry and Physics*, 2014, **14**, 3977–3989.
1300 95 J. F. Hunter, D. A. Day, B. B. Palm, R. L. N. Yatavelli, A. W. H. Chan, L. Kaser, L. Cappellin, P. L. Hayes, E.
1301 S. Cross, A. J. Carrasquillo, P. Campuzano-Jost, H. Stark, Y. Zhao, T. Hohaus, J. N. Smith, A. Hansel, T. Karl,
1302 A. H. Goldstein, A. Guenther, D. R. Worsnop, J. A. Thornton, C. L. Heald, J. L. Jimenez and J. H. Kroll,
1303 Comprehensive characterization of atmospheric organic carbon at a forested site, *Nature Geoscience*, 2017, **10**,
1304 748–753.
1305 96 K. H. Bates, D. J. Jacob, S. Wang, R. S. Hornbrook, E. C. Apel, M. J. Kim, D. B. Millet, K. C. Wells, X. Chen,
1306 J. F. Brewer, E. A. Ray, R. Commane, G. S. Diskin and S. C. Wofsy, The Global Budget of Atmospheric
1307 Methanol: New Constraints on Secondary, Oceanic, and Terrestrial Sources, *Journal of Geophysical Research:*
1308 *Atmospheres*, 2021, **126**, e2020JD033439.
1309 97 R. Holzinger, J. Williams, G. Salisburry, T. Klüpfel, M. de Reus, M. Traub, P. J. Crutzen and J. Lelieveld,
1310 Oxygenated compounds in aged biomass burning plumes over the Eastern Mediterranean: evidence for strong
1311 secondary production of methanol and acetone, *Atmospheric Chemistry and Physics*, 2005, **5**, 39–46.
1312 98 L. Hu, D. B. Millet, S. Y. Kim, K. C. Wells, T. J. Griffis, E. V. Fischer, D. Helmig, J. Hueber and A. J. Curtis,
1313 North American acetone sources determined from tall tower measurements and inverse modeling, *Atmos. Chem.*
1314 *Phys.*, 2013, **13**, 3379–3392.
1315 99 L. Hu, D. B. Millet, M. J. Mohr, K. C. Wells, T. J. Griffis and D. Helmig, Sources and seasonality of atmospheric
1316 methanol based on tall tower measurements in the US Upper Midwest, *Atmos. Chem. Phys.*, 2011, **11**, 11145–
1317 11156.
1318 100 S. Wang, E. C. Apel, R. H. Schwantes, K. H. Bates, D. J. Jacob, E. V. Fischer, R. S. Hornbrook, A. J. Hills, L.
1319 K. Emmons, L. L. Pan, S. Honomichl, S. Tilmes, J.-F. Lamarque, M. Yang, C. A. Marandino, E. S. Saltzman,
1320 W. de Bruyn, S. Kameyama, H. Tanimoto, Y. Omori, S. R. Hall, K. Ullmann, T. B. Ryerson, C. R. Thompson,
1321 J. Peischl, B. C. Daube, R. Commane, K. McKain, C. Sweeney, A. B. Thames, D. O. Miller, W. H. Brune, G. S.
1322 Diskin, J. P. DiGangi and S. C. Wofsy, Global Atmospheric Budget of Acetone: Air-Sea Exchange and the
1323 Contribution to Hydroxyl Radicals, *Journal of Geophysical Research: Atmospheres*, 2020, **125**, e2020JD032553.
1324 101 K. C. Wells, D. B. Millet, L. Hu, K. E. Cady-Pereira, Y. Xiao, M. W. Shephard, C. L. Clerbaux, L. Clarisse, P.-
1325 F. Coheur, E. C. Apel, J. de Gouw, C. Warneke, H. B. Singh, A. H. Goldstein and B. C. Sive, Tropospheric

1326 methanol observations from space: retrieval evaluation and constraints on the seasonality of biogenic emissions,
1327 *Atmospheric Chemistry and Physics*, 2012, **12**, 5897–5912.
1328